Staphylococcus aureus–induced endothelial permeability and inflammation are mediated by microtubule destabilization

Received for publication, May 17, 2018, and in revised form, December 13, 2018 Published, Papers in Press, January 8, 2019, DOI 10.1074/jbc.RA118.004030

Pratap Karki[‡], Yunbo Ke[§], Yufeng Tian[¶], Tomomi Ohmura[¶], Albert Sitikov[¶], Nicolene Sarich[¶], Christopher P. Montgomery[¶‖], and Anna A. Birukova[‡1]

From the [‡]Division of Pulmonary and Critical Care Medicine, Department of Medicine, University of Maryland School of Medicine, Baltimore, Maryland 21201, the [§]Department of Anesthesiology, University of Maryland School of Medicine, Baltimore, Maryland 21201, the [¶]Section of Pulmonary and Critical Care Medicine, Department of Medicine, University of Chicago, Chicago, Illinois 60637, and the [‖]Department of Critical Care Medicine, Nationwide Children's Hospital, Columbus, Ohio 43205

Edited by Velia M. Fowler

Staphylococcus aureus **is a major etiological agent of sepsis and induces endothelial cell (EC) barrier dysfunction and inflammation, two major hallmarks of acute lung injury. However, the molecular mechanisms of bacterial pathogen–induced EC barrier disruption are incompletely understood. Here, we investigated the role of microtubules (MT) in the mechanisms of EC barrier compromise caused by heat-killed *S. aureus* (HKSA). Using a customized monolayer permeability assay in human pulmonary EC and MT fractionation, we observed that HKSA-induced barrier disruption is accompanied by MT destabilization and increased histone deacetylase-6 (HDAC6) activity resulting from elevated reactive oxygen species (ROS) production. Molecular or pharmacological HDAC6 inhibition rescued barrier function in HKSA-challenged vascular endothelium. The HKSA-induced EC permeability was associated with impaired MT-mediated delivery of cytoplasmic linker–associated protein 2 (CLASP2) to the cell periphery, limiting its interaction with adherens junction proteins. HKSA-induced EC barrier dysfunction was also associated with increased Rho GTPase activity via activation of MT-bound Rho-specific guanine nucleotide exchange factor-H1 (GEF-H1) and was abolished by HDAC6 down-regulation. HKSA activated the NF-κB proinflammatory pathway and increased the expression of intercellular and vascular cell adhesion molecules in EC, an effect that was also HDAC6-dependent and mediated, at least in part, by a GEF-H1/Rho-dependent mechanism. Of note, HDAC6 knockout mice or HDAC6 inhibitor–treated WT mice were partially protected from vascular leakage and inflammation caused by both HKSA or methicillin-resistant *S. aureus* (MRSA). Our results indicate that *S. aureus*–induced, ROS-dependent up-regulation of HDAC6 activity destabilizes MT and thereby activates the GEF-H1/Rho pathway, increasing both EC permeability and inflammation.**

Staphylococcus aureus (SA)[2] infections are the predominant cause of sepsis, which is still the twelfth leading cause of death in the U. S. population. Severe sepsis is the most common cause of mortality among critically ill patients in noncoronary intensive care units (1, 2). Both sepsis and SA-induced pneumonia are major contributors in the development of acute lung injury (ALI) and its life-threatening complication, acute respiratory distress syndrome (3). Antibiotic therapy is provided to treat SA infections, but the pathogenesis associated with killed bacterium and widespread emergence of drug-resistant species such as methicillin-resistant SA (MRSA) remain a daunting challenge. MRSA infection is a major cause (38%) of ventilator-associated pneumonia in surgical intensive care units, and a large population of MRSA pneumonia develops severe sepsis and septic shock (4, 5).

Cellular wall components of SA, peptidoglycan G and lipoteichoic acid, are potent activators of endothelial permeability and inflammation, which drive acute respiratory distress syndrome (6, 7). We demonstrated previously that heat-killed SA (HKSA) increases permeability in cultured human pulmonary endothelial cells (HPAEC) and induces vascular leakage and inflammation in mice (8). Detrimental effects of SA on pulmonary endothelium can be triggered by the activation of p38 and Erk1/2 MAP kinases, NF-κB inflammatory cascade, and small GTPase RhoA (6). Our recent report suggests an important role of microtubule (MT) dynamics in the regulation of SA-induced endothelial dysfunction and inflammation (9).

The small GTPases RhoA, Rac1, and Rap1 play an active role in vascular endothelial cytoskeletal remodeling and the regulation of endothelial barrier integrity (10). These GTPases act as a molecular switch by cycling between GTP-bound active and

This work was supported by National Institutes of Health Grants HL107920 and HL130431 from NHLBI and GM114171 from NIGMS. The authors declare that they have no conflicts of interest with the contents of this article. The content is solely the responsibility of the authors and does not necessarily represent the official views of the National Institutes of Health.

[1] To whom correspondence should be addressed: Pulmonary and Critical Care Medicine, University of Maryland School of Medicine, 20 Penn St., HSF-2, Rm. S143, Baltimore, MD 21201. Tel.: 410-706-2545; Fax: 410-706-6952; E-mail: abirukova@som.umaryland.edu.

[2] The abbreviations used are: SA, *Staphylococcus aureus*; ALI, acute lung injury; MRSA, methicillin-resistant *S. aureus*; HKSA, heat-killed *S. aureus*; HPAEC, human pulmonary artery endothelial cell(s); MT, microtubule(s); EC, endothelial cell(s); ICAM, intercellular adhesion molecule; VCAM, vascular cell adhesion molecule; GEF-H1, guanine nucleotide exchange factor H1; HDAC, histone deacetylase(s); LPS, lipopolysaccharide; CLASP2, cytoplasmic linker–associated protein 2; TER, transendothelial electrical resistance; VE-cadherin, vascular endothelial cadherin; AJ, adherens junction; ROS, reactive oxygen species; TubA, tubastatin A; CD, catalytically deficient; BAL, bronchoalveolar lavage; KO, knockout; HSP90, heat shock protein 90; GAPDH, glyceraldehyde-3-phosphate dehydrogenase; TLR, Toll-like receptor; MLC, myosin light chain; ANOVA, analysis of variance; DAPI, 4′,6-diamidino-2-phenylindole.

GDP-bound inactive states. The activation of RhoA triggers endothelial cell (EC) barrier disruption and promotes inflammation. The Rho pathway of EC permeability involves the phosphorylation and inactivation of myosin phosphatase by Rho-associated kinase resulting in increased levels of phosphorylated regulatory myosin light chains and actomyosin contractility (reviewed in Ref. 11). On the other hand, Rho signaling further activates the NF-κB signaling cascade leading to increased expression of EC adhesion molecules including intercellular adhesion molecule-1 (ICAM-1), EC-specific vascular cell adhesion molecule-1 (VCAM-1), and inflammatory cytokines IL-6, IL-1β, and IL-8, ultimately resulting in augmented inflammation (12–14).

The MT cytoskeleton plays a critical role in the control of cell division and intracellular trafficking of organelles and proteins. Increasing evidence suggests that MT also play an active role in the regulation of endothelial permeability via cross-talk with the actin cytoskeleton (15, 16). MT cycle between polymerized and depolymerized states, which is determined by post-translational modifications such as the acetylation/deacetylation of tubulin and by numerous MT-associated proteins (17). A plethora of studies have documented that MT destabilization induced by various agonists impairs endothelial function by activating the Rho pathway (18–23). Indeed, MT may directly regulate Rho activity via guanine nucleotide exchange factor H1 (GEF-H1), whose activity is suppressed if GEF-H1 is in the MT-bound state. Once released from the MT during MT disassembly, GEF-H1 activates Rho (24, 25).

Furthermore, histone deacetylase 6 (HDAC6), a member of the class II HDAC, has emerged as a key regulator of MT dynamics (26, 27). A role for HDAC6 in MT-dependent endothelial dysfunction was initially suggested by findings that HDAC6 activity promotes the destabilization of MT by deacetylating α-tubulin, whereas inhibition of HDAC6 attenuates lung dysfunction caused by thrombin or lipopolysaccharide (LPS) (28–30). A similar pattern of endothelial barrier protection has also been achieved using the MT-stabilizing agent, Taxol (31, 32). However, the precise role of MT and the molecular/cellular mechanisms involved in bacterial pathogen–induced endothelial barrier dysfunction and inflammation remains to be investigated.

Cytoplasmic linker–associated protein 2 (CLASP2) is a MT plus-end tracking protein that promotes the stabilization of dynamic microtubules (33). CLASP2 is directly involved in MT–actin cytoskeleton interactions (34) and MT stabilization at the cell cortex (35). The regional immobilization of CLASP2 allows MT stabilization and promotes directionally persistent fibroblast and epithelial cell motility (35). CLASP2 interaction with adherens junction protein p120 catenin observed in keratinocytes (36, 37) suggests its additional role in linking MT with cell junction complexes. These features suggest that CLASP2 is a potentially important regulator of MT–actin cytoskeleton cross-talk and EC barrier regulation.

In this study, we explored the role of MT dynamics in HKSA-induced endothelial barrier dysfunction and lung inflammation. By employing molecular and pharmacological inhibitors, we elucidated the mechanisms of HKSA-induced activation of HDAC6 that cause MT destabilization and MT-dependent signaling, leading to increased endothelial permeability and vascular inflammation. We also evaluated the protective effects of HDAC6 inhibition as a potential therapeutic for HKSA or MRSA-induced vascular leak and inflammation *in vivo*.

Results

HKSA-induced EC barrier disruption is accompanied by MT destabilization

Our earlier study showed that the destabilization of MT mediates EC dysfunction caused by Gram-positive bacteria–derived peptidoglycan G (9). We further investigated the MT-dependent mechanism of EC permeability and inflammation caused by HKSA. HKSA robustly increased endothelial permeability in a dose-dependent fashion, as reflected by decreased transendothelial electrical resistance (TER) (Fig. 1*A*). We also analyzed the effect of HKSA on EC monolayer macromolecular permeability using a permeability assay developed by our group (38) and described under "Experimental procedures." HKSA increased in a dose-dependent manner the permeability of the human pulmonary EC monolayer for a FITC–dextran tracer (Fig. 1*B*). To evaluate the effects of an HKSA challenge on MT dynamics, we performed a MT fractionation assay that investigated HKSA-induced changes in the pools of polymerized and depolymerized tubulin. The results showed that HKSA treatment markedly decreased the pool of polymerized MT, suggesting increased MT disassembly (Fig. 1*C*).

HKSA increases HDAC6 activity in a redox-dependent fashion

We further investigated the mechanism of HKSA-induced MT destabilization mediating HKSA-induced EC permeability. Acetylation of tubulin confers increased MT stability (39). HKSA treatment markedly decreased the pool of acetylated tubulin-positive MT in pulmonary EC detected by immunofluorescence staining with acetylated tubulin-specific antibody (Fig. 2*A*). Combined visualization of acetylated tubulin and VE-cadherin–positive intercellular junctions shows coordinated decline in acetylated tubulin and VE-cadherin immunoreactivity in HKSA-challenged EC (Fig. 2*B*). Imaging data were further confirmed by Western blot analysis of total cell lysates from control and HKSA-challenged EC. The results show a sustained decrease of acetylated tubulin in the total tubulin pool (Fig. 2C).

HDAC6, a member of the HDAC family, is localized in cytosol and has been shown to deacetylate MT (30). We examined whether HDAC6 was involved in HKSA-induced EC dysfunction. Using a biochemical HDAC6 activation assay, we found that HKSA indeed increased HDAC6 activity (Fig. 2*D*). HKSA-induced HDAC6 activation was attenuated by the reactive oxygen species (ROS) scavengers *N*-acetylcysteine and amifostine, an FDA-approved compound with reported antioxidant properties (40) (Fig. 2*D*).

Inhibition of HDAC6 attenuates HKSA-induced EC barrier disruption

To further evaluate the role of HDAC6 in HKSA-induced endothelial barrier disruption, we employed pharmacological and molecular inhibitors of HDAC6. EC pretreatment with the HDAC6-specific inhibitor tubastatin A (TubA) completely abolished the HKSA-induced decrease in the pool of acetylated

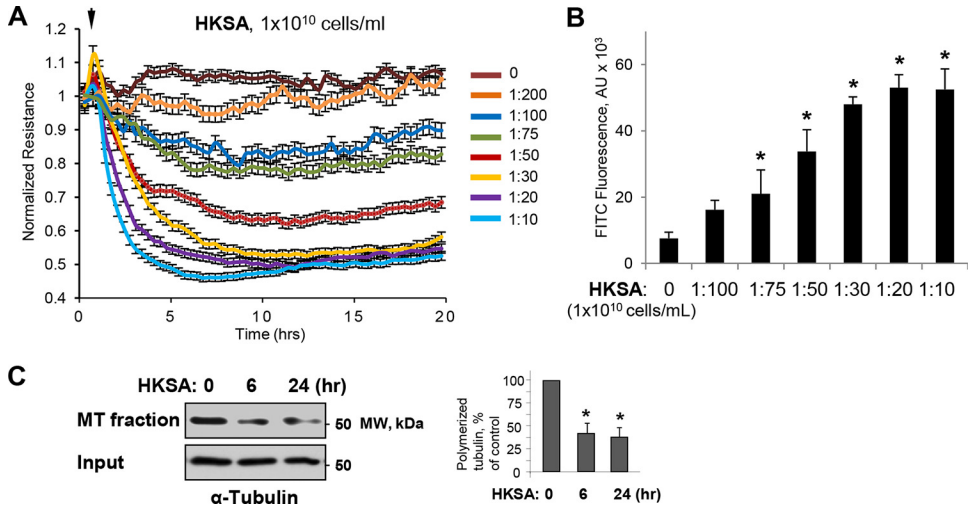

Figure 1. HKSA-induced EC permeability is accompanied by MT destabilization. *A*, HPAEC monolayers grown on gold microelectrodes were challenged with the indicated concentrations of HKSA, and TER was monitored for 20 h. *B*, cells grown on 96-well plates with immobilized biotinylated gelatin were exposed to HKSA for 2 h. After completion of stimulation, FITC–avidin (25 μg/ml) was added to the cells, and they were incubated for 3 min followed by washing with PBS and measurement of FITC fluorescence in a Victor X5 plate reader. Normalized values are expressed as mean ± S.D.; $n = 6$, *, $p < 0.05$. *C*, MT fractionation from control and HKSA-treated (2×10^8 particles/ml, 6 or 24 h) EC was performed by separation of soluble depolymerized tubulin and insoluble tubulin polymers assembled into MT by centrifugation as described under "Experimental procedures." Densitometry results are shown as mean ± S.D. $n = 5$; *, $p < 0.05$.

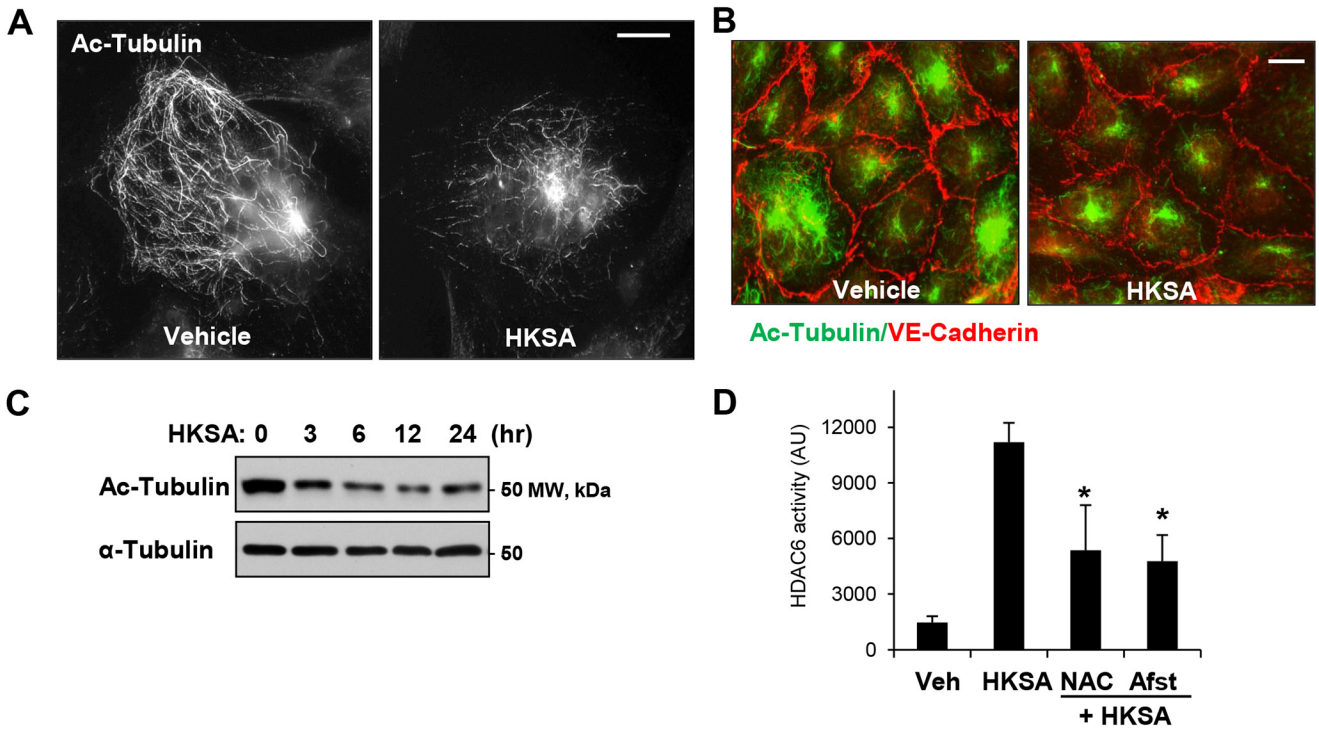

Figure 2. HKSA decreases the pool of acetylated microtubules and increases HDAC activity in a redox-dependent manner. *A*, the levels of acetylated MT in control and HKSA-treated (2×10^8 particles/ml, 6 h) cells were determined by immunofluorescence staining with acetylated tubulin antibody. *Bar* = 5 μm. *B*, co-staining of control and HKSA-stimulated (6 h) EC monolayers with antibodies to acetylated tubulin and VE-cadherin. VE-cadherin–positive adherens junctions outline the cell borders. Shown are representative results of three independent experiments. *Bar* = 10 μm. *C*, the total cell lysates collected from the cells were treated with HKSA for the indicated times, and acetylated tubulin levels in total cell lysates were analyzed by Western blotting (*upper panel*). *Lower panel*, shows total a-tubulin levels. Shown are representative results of three independent experiments. *D*, EC were stimulated with HKSA (3 h) followed by an HDAC6 activity assay. Where indicated, cells were pretreated for 30 min with the ROS scavenger *N*-acetylcysteine (*NAC*, 1 mM) or amifostine (*Afst*, amifostine trihydrate, WR2721, 4 mM). The results are presented after normalizing to background controls. *, $p < 0.05$; $n = 5$. *Veh*, vehicle.

tubulin as determined by Western blot analysis (Fig. 3*A*). Immunofluorescence staining of the microtubule cytoskeleton showed that HKSA induced partial disassembly of peripheral MT was abrogated by pretreatment with TubA (Fig. 3*B*). TubA also strongly attenuated HKSA-induced actin cytoskeletal remodeling by inhibiting the formation of paracellular gaps (Fig. 3*C*, marked by *arrows*). The efficacy of TubA in attenuating HKSA-induced EC barrier dysfunction was further demonstrated by monitoring TER changes in HKSA-stimulated EC monolayers. The HKSA-induced drop in resistance was

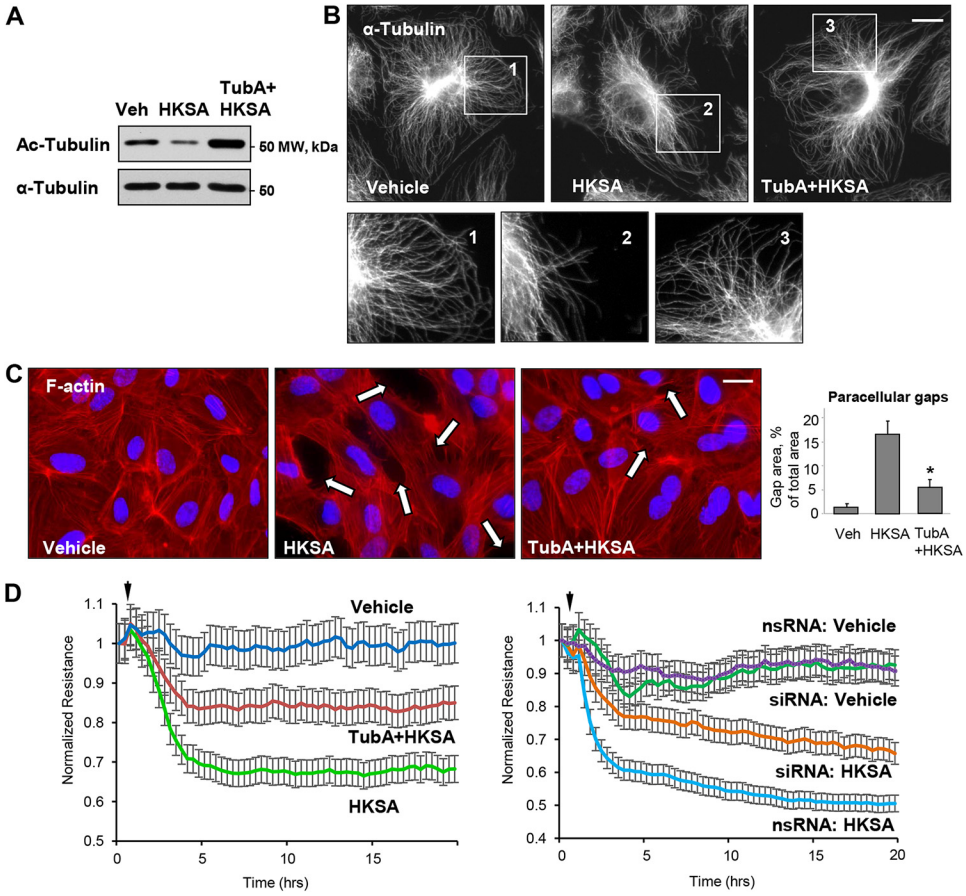

Figure 3. HDAC6 inhibitor attenuates HKSA-induced EC barrier dysfunction. HPAEC were treated with vehicle (*Veh*) or HDAC6 inhibitor TubA (10 μM, 30 min) followed by HKSA challenge (2×10^8 particles/ml, 6 h); MT integrity, actin cytoskeleton remodeling, and paracellular gap formation were monitored. *A*, *top*, acetylated tubulin levels were determined by Western blotting. *Bottom*, depicts total α-tubulin levels in samples. *B*, microtubule organization was monitored by immunofluorescence staining with α-tubulin antibody. The *outlined areas* in the *top row* (*inserts 1–3*) are depicted as corresponding higher-magnification images in the *bottom row*, revealing details of peripheral MT organization. *Bar* = 5 μm. *C*, cells were stained with Texas Red phalloidin to visualize F-actin. Cell nuclei were visualized by DAPI counterstaining. Paracellular gaps are shown by *arrows*; *bar* = 10 μm. Shown are representative results of three independent experiments. *Veh*, vehicle. *D*, cells were stimulated with HKSA (*arrowheads*) in the presence or absence of TubA (*left panel*), or they were transfected with HDAC6-specific or nonspecific siRNA prior to HKSA challenge (*right panel*). TER was monitored over a 20-h time period.

attenuated by EC pretreatment with TubA (Fig. 3*D*, *left*) or siRNA-mediated HDAC6 knockdown (Fig. 3*D*, *right*).

HKSA causes AJ disassembly and impairs interactions between MT and AJ proteins

To investigate the mechanism of HKSA-induced breakdown of cell junctions, we performed immunofluorescence staining of pulmonary EC with adherens junction protein VE-cadherin. HKSA treatment dramatically decreased VE-cadherin localization at cell–cell junctions and caused intercellular gap formation (Fig. 4*A*, shown by *arrows*). The HKSA-induced disappearance of VE-cadherin from cell–cell contacts was rescued by the HDAC6 inhibitor TubA (Fig. 4*A*). HKSA induced the disassembly of the VE-cadherin–p120 catenin complex as evidenced by co-immunoprecipitation assay and also caused a decrease in the VE-cadherin presence at the cell surface, as demonstrated by a surface protein biotinylation assay. After *in situ* biotinylation of cell surface proteins in control and stimulated EC monolayers, the level of biotinylated VE-cadherin was assessed by Western blotting. The HKSA-induced decrease of the VE-cadherin presence at the cell surface was attenuated by HDAC6 inhibitor (Fig. 4*B*). Reciprocal co-immunoprecipitation assays using VE-cadherin and p120 catenin antibodies showed that HKSA-induced dissociation of the VE-cadherin–p120 catenin protein complex was attenuated by TubA (Fig. 4*C*). The disappearance of VE-cadherin from the cell surface upon HKSA challenge may be caused by enhanced internalization, reduced recycling of VE-cadherin back to the cell surface, or both, and it ultimately leads to AJ disassembly and EC barrier compromise.

The interaction between the MT plus-end–binding protein CLASP2 and p120 catenin regulates MT dynamics at the AJ in keratinocytes (36). Using a surface protein biotinylation assay, we found that siRNA-specific knockdown of CLASP2 decreased the pool of biotinylated VE-cadherin, reflecting increased VE-cadherin internalization and AJ disassembly in pulmonary EC (Fig. 5*A*). These data suggest functional interactions between CLASP2 and the EC adherens junction complex. Interestingly, HKSA stimulation caused CLASP2 redistribution from the EC membrane/cytoskeletal fraction, suggesting CLASP2 disappearance from the EC cortical compartment (Fig. 5*B*). Western blotting *panels* (Fig. 5*B*, *right*) confirm the expression of cell membrane (VEGFR2 and Na^+/K^+-ATPase) and cytosolic (HSP90 and GAPDH) protein markers in the corresponding fractions.

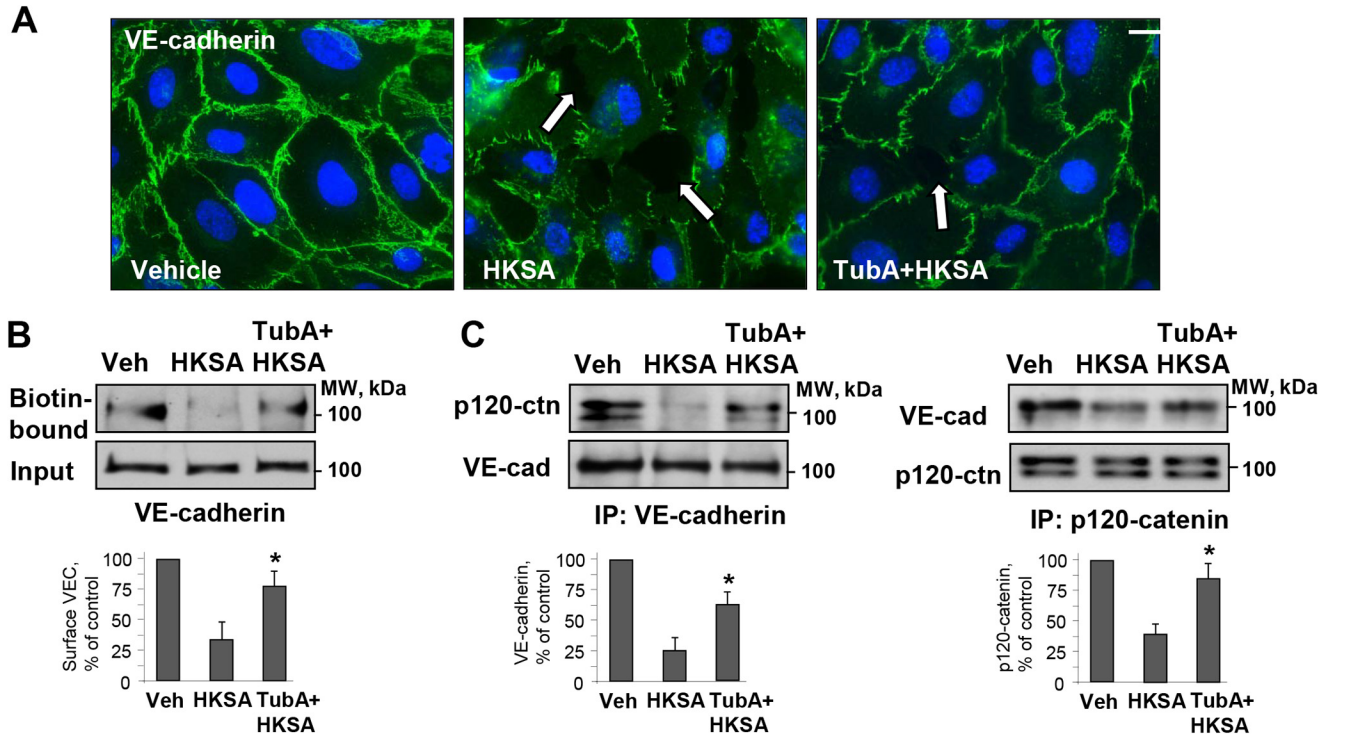

Figure 4. HDAC6 inhibitor rescues HKSA-induced cell junction breakdown by reversing compromised membrane targeting and interactions of adherens junction proteins. *A*, immunofluorescence staining of HPAEC with VE-cadherin antibody after HKSA challenge (2×10^8 particles/ml, 6 h) was performed to monitor cell junction remodeling. Cell nuclei were visualized by DAPI counterstaining; *bar* = 10 μm. Shown are representative results of three independent experiments. *B*, EC monolayers were treated with HKSA alone (4 h) or in combination with TubA, and a surface biotinylation assay was performed. *C*, reciprocal co-immunoprecipitation (*IP*) assays in similar experiments were performed with VE-cadherin antibody (*left*) or p120 antibody (*right*). Precipitated immunocomplexes were analyzed by Western blotting with the indicated antibodies. *Bar graphs* depict a quantitative analysis of Western blotting densitometry data. Results are shown as mean ± S.D. $n = 5$; *, $p < 0.05$. *Veh*, vehicle.

Co-immunoprecipitation assays using p120 catenin antibody showed the presence of CLASP2 in p120 catenin immunocomplexes, which was significantly decreased in the HKSA-treated group. Importantly, pharmacological inhibition of HDAC6 activity preserved CLASP2–p120 catenin interactions in HKSA-stimulated EC (Fig. 5*C*).

HKSA-induced EC inflammation is mediated by HDAC6

We next sought to determine whether HDAC6 plays a role in HKSA-induced EC inflammation. Activation of the NF-κB pathway is a central mechanism of the HKSA-induced EC inflammatory response reflected by increased NF-κB phosphorylation and nuclear translocation (41). We monitored phospho-NF-κB levels as a measure of NF-κB activation in HKSA-treated pulmonary EC. HKSA increased phospho-NF-κB levels, an effect that was attenuated by pharmacological inhibition of HDAC6 activity using TubA (Fig. 6*A*). Along with NF-κB phosphorylation, the degradation of the NF-κB inhibitory subunit, IkBα, is another indicator of NF-κB activation. The results showed that HKSA treatment decreased cellular levels of IkBα, an effect that was also blocked by the HDAC inhibitor (Fig. 6*A*). NF-κB activation leads to its nuclear translocation. Immunofluorescence analysis of NF-κB intracellular localization showed HKSA-induced NF-κB localization in the nuclei of stimulated cells, which was attenuated by TubA (Fig. 6*B*). EC adhesion molecules ICAM-1 and VCAM-1 are key regulators of the neutrophil recruitment at the sites of inflammation, and their expression is triggered by NF-κB pathway (42). HKSA caused potent up-regulation of ICAM-1 and VCAM-1 expression in pulmonary EC. This effect was suppressed by HDAC6 inhibitor TubA (Fig. 6*C*), which also abolished the HKSA-induced decrease in acetylated tubulin (Fig. 6*C*, *bottom panel*). Similarly, HKSA-induced ICAM-1 and VCAM-1 expression was attenuated by molecular inhibition of HDAC6 using gene-specific siRNA (Fig. 6*D*). HDAC6 inhibition also suppressed the HKSA-induced production of inflammatory cytokines IL-6 and IL-8 and soluble ICAM1 by HKSA-stimulated pulmonary EC (Fig. 6*E*).

To test directly the role of HDAC6 activity in HSKA-induced EC inflammation, we overexpressed WT HDAC6 and the catalytically deficient (CD) HDAC6 mutant and determined the levels of phospho-NF-κB, ICAM-1, and VCAM-1 in HKSA-challenged pulmonary EC. Although HKSA caused pronounced NF-κB phosphorylation in EC with ectopic expression of WT HDAC6, the NF-κB phosphorylation response was abrogated in pulmonary EC with ectopic expression of the catalytically inactive HDAC6 (CD-HDAC6) mutant (Fig. 6*F*). In line with its effects on NF-κB phosphorylation, ectopic expression of the CD-HDAC6 mutant suppressed HKSA-induced expression of ICAM-1 and VCAM-1 (Fig. 6*F*).

HKSA-induced EC inflammation is mediated by MT-bound GEF-H1 and Rho activation

The activation of RhoA GTPase signaling plays an essential role in mediating both EC permeability and inflammation (10).

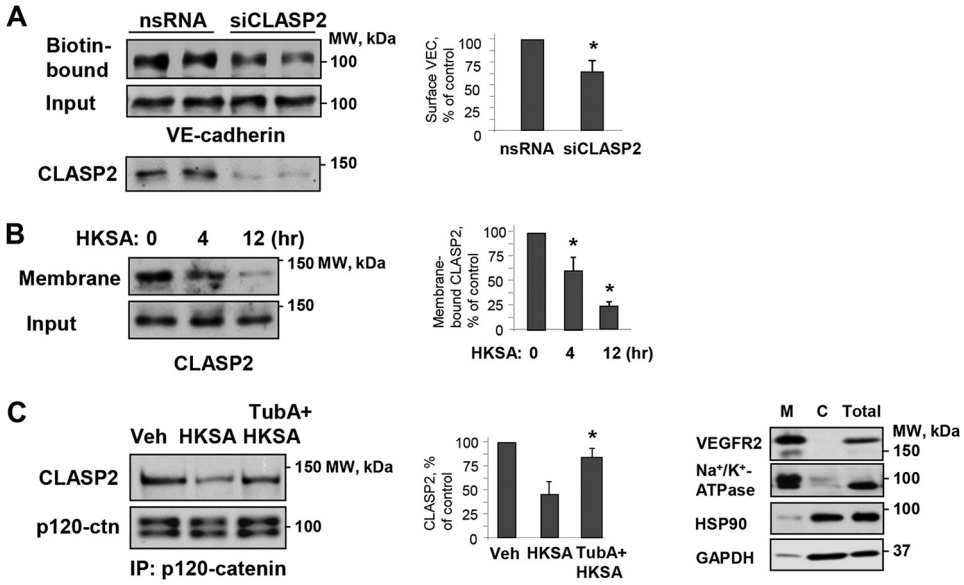

Figure 5. Role of MT plus-end–binding protein CLASP2 and microtubules in modulation of HKSA-induced cell junction dysfunction. *A*, HPAEC were transfected with CLASP2-specific (*siCLASP2*) or nonspecific siRNA (*nsRNA*) for 72 h, and a surface protein biotinylation assay was performed for VE-cadherin. The efficiency of endogenous CLASP2 knockdown was confirmed by membrane reprobing with CLASP2 antibody. *B*, cells were treated with HKSA (4 h), and membrane/cytoskeletal fractions were analyzed by Western blotting to monitor redistribution of CLASP2. Equal protein amounts of corresponding total cell lysates were loaded and additionally probed for CLASP2 to ensure equal input protein. The results of Western blot analysis (*right panel*) confirm the expression of cell membrane (VEGFR2 and Na^+/K^+-ATPase) and cytosolic (HSP90 and GAPDH) protein markers in the corresponding fractions. *C*, cells were challenged with HKSA (4 h) with or without pretreatment with TubA, and co-immunoprecipitation was performed with p120 antibody followed by immunoblotting with CLASP2. The membrane was reprobed with p120 antibody to ensure even pulldown among the groups. *Bar graphs* depict a quantitative analysis of Western blotting densitometry data. Results are shown as mean ± S.D. $n = 5$; *, $p < 0.05$. *Veh*, vehicle.

Furthermore, MT may directly modulate the Rho pathway via MT-bound RhoA-specific guanine nucleotide exchange factor GEF-H1 (25). In this context, we investigated whether HKSA induces Rho activation via the MT–GEF-H1 mechanism. HKSA treatment increased GEF-H1 activity as evaluated by the GEF-H1 activation pulldown assay described under "Experimental procedures." GEF-H1 activation was attenuated by siRNA-induced HDAC6 knockdown (Fig. 7*A*). Activation of the GEF-H1–RhoA pathway in HKSA-stimulated EC was further reflected by increased Rho kinase-specific phosphorylation of myosin phosphatase and increased phosphorylation of the regulatory myosin light chain (Fig. 7*B*). These effects were attenuated by HDAC6 knockdown.

To verify the role of MT-bound GEF-H1 in mediating HKSA-induced inflammation, we employed GEF-H1 gene–specific siRNA to deplete GEF-H1 endogenous expression. The results show that depletion of GEF-H1 suppressed the HKSA-induced NF-κB phosphorylation. Likewise, GEF-H1 knockdown attenuated the HKSA-induced expression of VCAM-1 (Fig. 7*C*).

HDAC6 inhibition prevents HKSA-induced lung inflammation in vivo

The protective effects of the HDAC6 inhibitor TubA were further tested in the murine model of HKSA-induced lung injury. Mice challenged with HKSA developed prominent acute lung injury with increased total cell counts and protein content in bronchoalveolar lavage (BAL) fluid (Fig. 8*A*). The pathologic effects of HKSA were significantly attenuated in the TubA-treated groups.

The lung vascular leak evaluated by Evans Blue extravasation into the lung parenchyma demonstrated a pronounced accumulation of the dye in the lungs of HKSA-challenged mice, which was markedly attenuated by i.v. injection of HDAC6 inhibitor (Fig. 8*B*). We also employed a noninvasive fluorescence imaging tool to monitor HKSA-induced vascular leak in the same animals on different days. The accumulation of an intravenously injected Angiosense 680 EX tracer in mice lungs reflects lung vascular leak, and clearance of the tracer from the lungs corresponds to vascular barrier recovery. HKSA-challenged mice showed an accumulation of the tracer with maximal accumulation at day 1, a gradual decline on days 2 and 3, and recovery by day 6. Intravenous administration of TubA markedly decreased the initial accumulation of the tracer, leading to accelerated recovery indicated by faster clearance of the tracer from the lungs (Fig. 8*C*).

The role of HDAC6 in septic ALI was further evaluated using a genetic model of HDAC6 knockout (KO) mice. HKSA-induced lung injury in HDAC6 KO mice and matching controls was monitored by analyzing the protein content and cell counts in BAL samples, along with extravasation of Evans Blue tracer into lung parenchyma. The results show that BAL parameters of HKSA-induced ALI cell counts and protein content (Fig. 9*A*), as well as HKSA-induced Evans Blue accumulation in the lung parenchyma (Fig. 9*B*) reflecting lung vascular leak, were significantly attenuated in HDAC6 KO mice as compared with matching WT controls. Consistently, noninvasive optical imaging of HKSA-injured lungs over 6 days post-challenge showed that HKSA induced an accumulation in the lung of an intravenously injected fluorescent probe (Angiosense) in WT mice, reflecting lung injury and barrier dysfunction. Lung injury was significantly attenuated in HDAC6 KO mice (Fig. 9*C*).

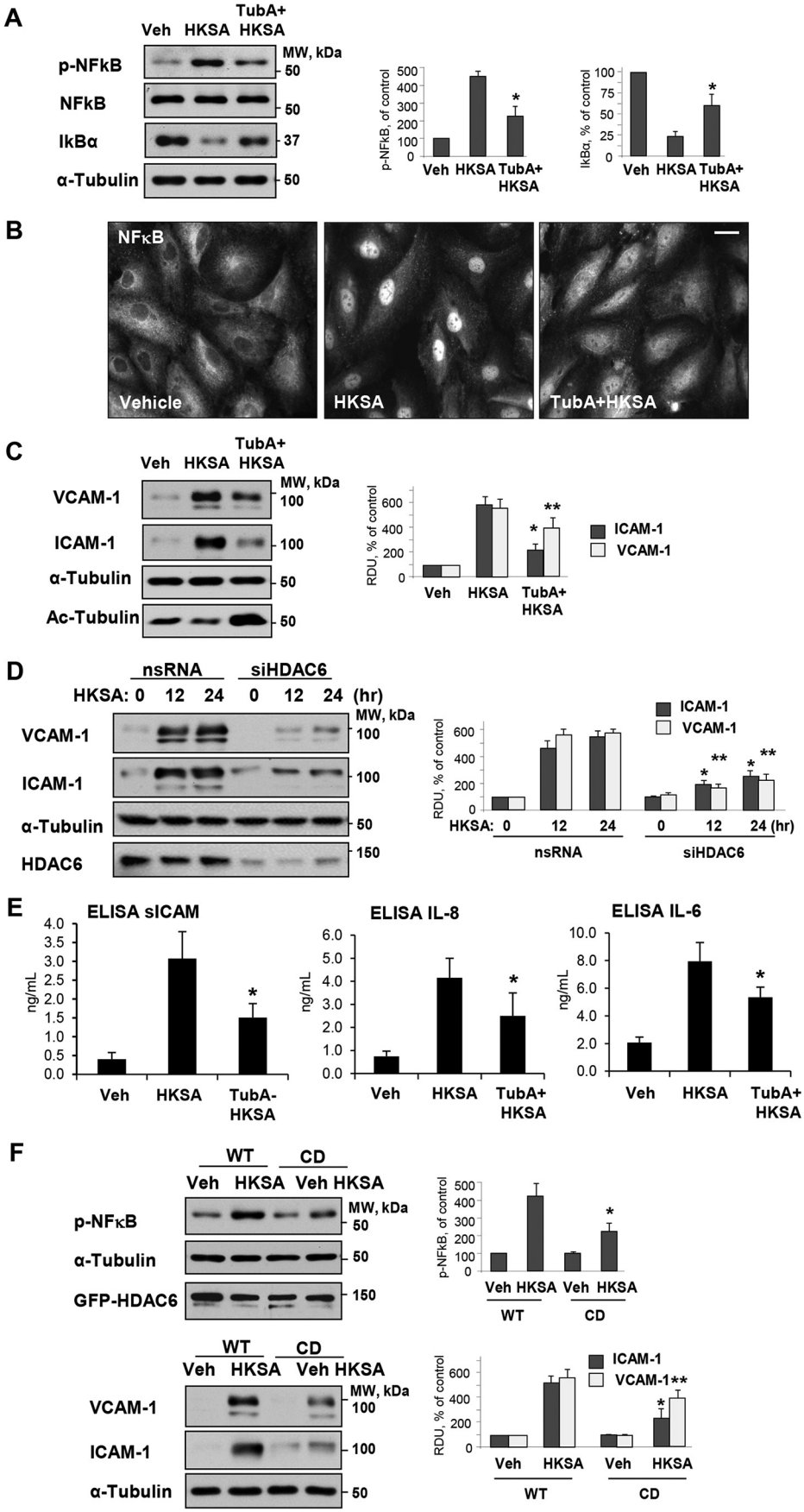
A
Veh
HKSA
TubA+ HKSA
MW, kDa
p-NFkB
NFkB
IkBα
α-Tubulin
50
50
37
50
p-NFkB, of control
IkBα, % of control
B
NFκB
Vehicle
HKSA
TubA+HKSA
C
VCAM-1
ICAM-1
α-Tubulin
Ac-Tubulin
100
100
50
50
RDU, % of control
ICAM-1
VCAM-1
D
nsRNA
siHDAC6
HKSA: 0 12 24 0 12 24 (hr)
VCAM-1
ICAM-1
α-Tubulin
HDAC6
100
100
50
150
RDU, % of control
HKSA: 0 12 24 0 12 24 (hr)
nsRNA
siHDAC6
E
ELISA sICAM
ELISA IL-8
ELISA IL-6
ng/mL
Veh
HKSA
TubA- HKSA
TubA+ HKSA
F
WT
CD
Veh HKSA Veh HKSA
p-NFκB
α-Tubulin
GFP-HDAC6
VCAM-1
ICAM-1
α-Tubulin
p-NFkB, of control
RDU, % of control
WT
CD

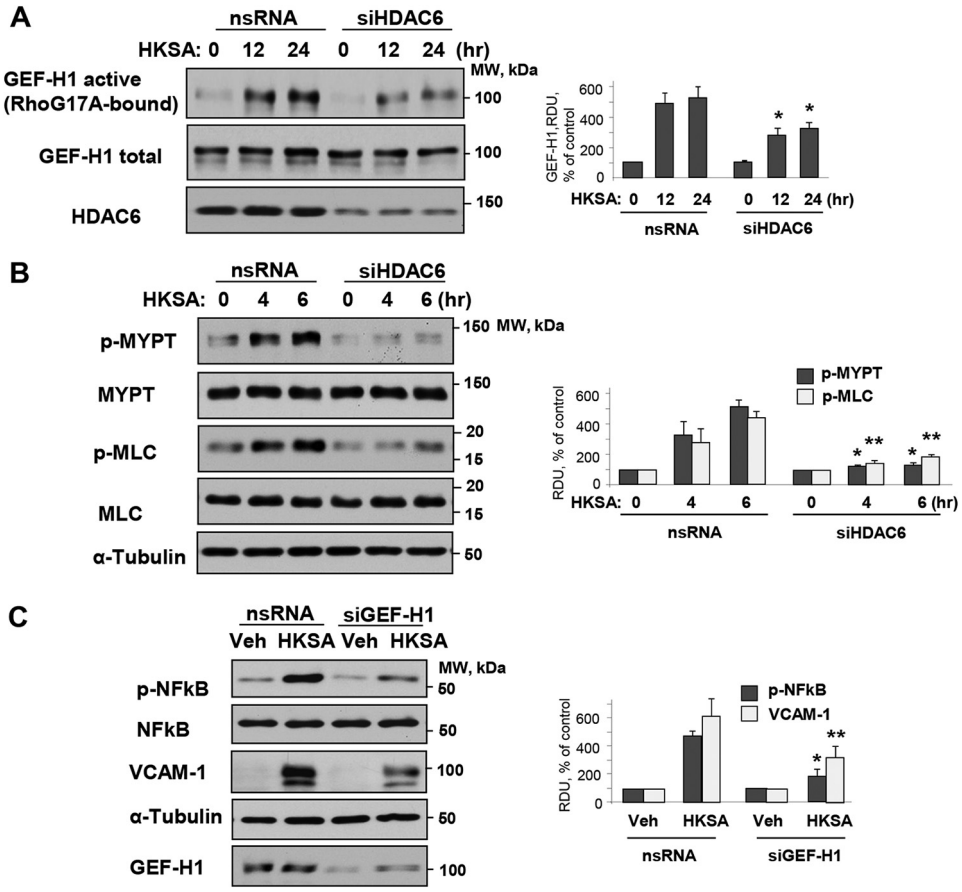

Figure 7. MT-bound GEF-H1 dependent Rho activation mediates HKSA-induced EC barrier disruption and inflammation. HPAEC transfected with HDAC6-specific (*siHDAC6*) or nonspecific siRNA (*nsRNA*) were exposed to HKSA for the indicated times. *A*, a GEF-H1 activation assay was performed with RhoG17A beads, and active GEF-H1 captured by the beads were detected by Western blotting. The efficiency of HDAC6 knockdown was confirmed by Western blotting of total cell lysates with HDAC6 antibody. *B*, phosphorylation of MLC and myosin phosphatase (*MYPT*) in total cell lysates was detected by Western blotting with corresponding phosphospecific antibodies. Membranes were then reprobed with pan-MYPT (*p-MYT*) and pan-MLC (*p-MLC*) antibodies. *C*, HPAEC were transfected with GEF-H1–specific or nonspecific siRNA and challenged with HKSA 72 h after transfection. The levels of phospho-NF-κB (HKSA 6 h) and VCAM-1 (HKSA 24 h) were evaluated by Western blotting. Equal total protein amounts were loaded on each lane; probing with α-tubulin was used as a confirmatory normalization control. *Bar graphs* depict a quantitative analysis of Western blotting densitometry data and shown as mean ± S.D. $n = 5$; *, $p <$ 0.05. *Veh*, vehicle.

Considering the emerging severity of antibiotic-resistant infections, we also investigated whether HDAC6 inhibition could prevent lung injury caused by inoculation with a live MRSA strain. Mice were pretreated i.v. with TubA (40 mg/kg) prior to MRSA inoculation (CR-MRSA USA300, clinical strain 923) followed by analysis of lung injury parameters 16 h after MRSA injection. The results show that pretreatment with the HDAC6 inhibitor attenuated the increase in BAL total cell counts and protein content in MRSA-treated mice (Fig. 10*A*), and reduced Evans Blue extravasation (Fig. 10*B*). BAL from MRSA-treated mice showed elevated levels of soluble ICAM-1 and inflammatory cytokine KC, which were reduced in the HDAC6 inhibitor-treated groups (Fig. 10*C*).

Discussion

SA infections, with their role in a wide range of pathologies from pneumonia to sepsis, represent an emerging and serious global concern. The widespread occurrence of antibiotic-re-

Figure 6. HDAC6 inhibition prevents HKSA-induced EC inflammation. *A*, HPAEC were treated with HKSA in the presence or absence of TubA, and the levels of phospho-NF-κB, total NF-κB, and IκBα in cell lysates were detected by Western blot analysis. Equal total protein amounts were loaded on each lane; probing with α-tubulin was used as a confirmatory normalization control. *Bar graphs* depict quantitative densitometry analysis of phospho-NF-κB and IκBα levels. Results are shown as mean ± S.D.; $n = 3$, *, $p < 0.05$. *B*, HKSA-induced nuclear translocation of NF-κB (6 h) was evaluated by immunofluorescence staining with NF-κB antibody. *Bar* = 10 μm. Shown are representative images of three independent experiments. *C*, VCAM-1 and ICAM-1 expression in total cell lysates from HKSA-stimulated (24 h) HPAEC monolayers was monitored by Western blotting. Equal total protein amounts were loaded on each lane; membrane reprobing with α-tubulin antibody was used as an additional normalization control. Reprobing with antibody to acetylated tubulin was used to evaluate the efficacy of TubA to inhibit α-tubulin deacetylation. *D*, cells were transfected with HDAC6-specific or nonspecific siRNA followed by stimulation with HKSA for the indicated times and detection of VCAM-1 and ICAM-1 expression by Western blotting. *Bar graphs* depict a quantitative analysis of Western blotting densitometry data. Results are shown as mean ± S.D. $n = 5$; *, $p < 0.05$. *E*, cells were exposed to HKSA (24 h) with or without pretreatment with TubA, and levels of soluble ICAM (*sICAM*), IL-8, and IL-6 in conditioned medium were analyzed by ELISA. *, $p < 0.05$; $n = 4$. *F*, HPAEC were transfected with plasmids encoding GFP-tagged WT or CD-HDAC6 mutant followed by stimulation with HKSA at 24 h post-transfection. Phospho-NF-κB (*top*) or VCAM-1 and ICAM-1 (*bottom*) levels were determined by Western blotting. Equal total protein amounts were loaded on each lane; probing with α-tubulin was used as a confirmatory normalization control. Ectopic expression of HDAC6 constructs was verified by probing with GFP antibody. *Bar graphs* depict a quantitative analysis of Western blotting densitometry data and shown as mean ± S.D. $n = 5$; * $p < 0.05$. *Veh*, vehicle.

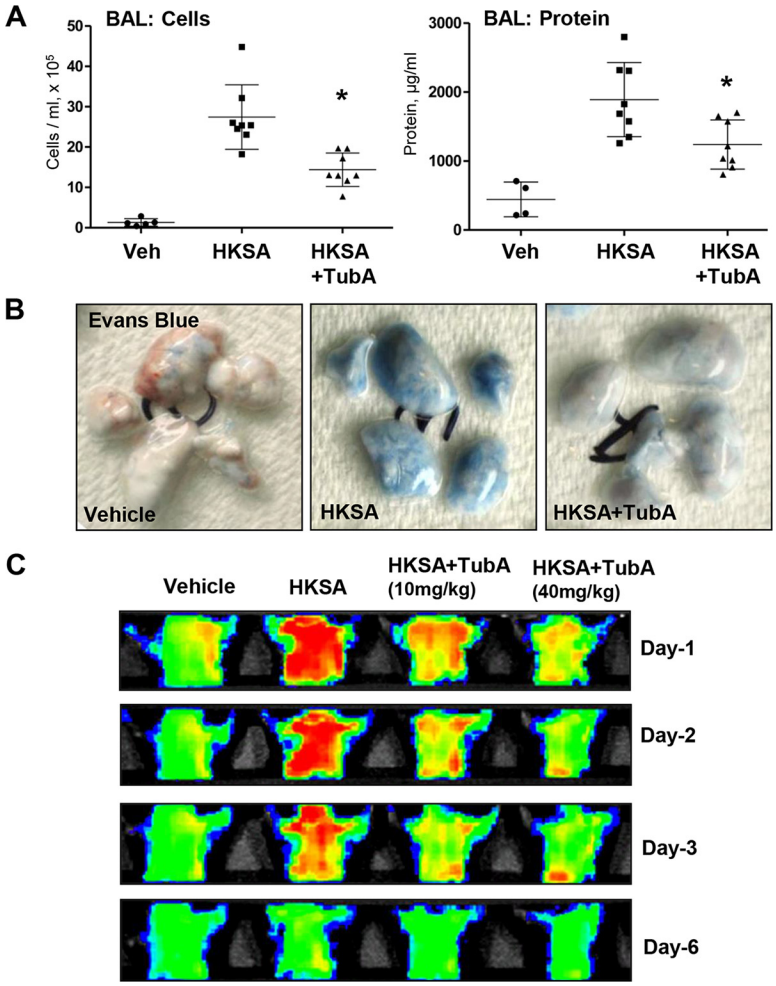

Figure 8. HDAC6 inhibition prevents HKSA-induced vascular leak and lung inflammation *in vivo*. Anesthetized mice were injected with HKSA (intratracheally, 2×10^8 bacterial cells/mouse) followed by intravenous injection of TubA. *A*, total cells and the protein content in BAL were determined 24 h after HKSA administration. $n = 8$; *, $p < 0.05$. *Veh*, vehicle. *B*, analysis of Evans Blue–labeled albumin extravasation into the lung parenchyma reflecting vascular leak. Lungs were excised from the chest, perfused with PBS, and imaged. Shown are representative single-animal images from three independent experiments. Nine total animals/condition were analyzed. *C*, live imaging analysis of lung vascular barrier dysfunction after HKSA intratracheal injection with and without intravenous administration of the indicated doses of TubA. HKSA-induced accumulation of fluorescent Angiosense 680 EX imaging agent in the lungs of the same animals was detected using the Xenogen IVIS 200 Spectrum imaging system at 1, 2, 3, and 6 days after HKSA challenge and presented in arbitrary *colors*. Shown are representative single-animal images from three independent experiments. Nine total animals/condition were analyzed.

sistant SA isolates such as MRSA has led to an urgent need for alternative approaches to combat these infections. In this study, we unraveled an important role of MT-associated signaling in SA-induced endothelial permeability and inflammation.

As the role of actin cytoskeletal remodeling in the regulation of endothelial permeability is well recognized, yet growing evidence suggests that MT dynamics also have a major impact on both endothelial barrier function and inflammatory activation (16, 19, 43, 44). Studies by different groups including our own have shown that barrier disruptive agonists thrombin, TNFα, LPS, and HKSA cause MT destabilization leading to endothelial barrier dysfunction (9, 18, 20, 45). Accordingly, MT-stabilizing drugs such as Taxol reverse these pathologic responses. This study shows that HKSA-induced pulmonary EC permeability and inflammation is associated with destabilization of the MT cytoskeleton caused by HKSA-induced activation of HDAC6 enzymatic activity, which has not been shown previously. The activation of ROS production in vascular endothelium triggered by Gram-positive and Gram-negative bacterial compounds has been linked previously to EC dysfunction (46, 47), although specific signaling mechanisms were not completely understood. Importantly, our data show that HKSA-induced HDAC6 activation is blunted in the presence of ROS inhibitors *N*-acetylcysteine and amifostine. This novel finding supports the redox-dependent mechanism of HDAC6-mediated regulation of EC permeability and inflammation via destabilization of the MT cytoskeleton in the HKSA model of ALI. The redox-dependent mechanism of HDAC6 activation may involve additional intermediate steps such as HDAC6 phosphorylation. For example, a recent study demonstrates that cigarette smoking-induced endothelial dysfunction and priming to ALI can be mediated by oxidative stress–activated glycogen synthase kinase 3β (GSK-3β), which then activates HDAC6 via phosphorylation of serine 22 leading to α-tubulin deacetylation (48). Redox-dependent MT disassembly has been also described in the settings of Gram-negative ALI caused by LPS (19). Taken together, these findings suggest a universal mechanism of MT-dependent EC dysfunction caused by bacterial pathogens.

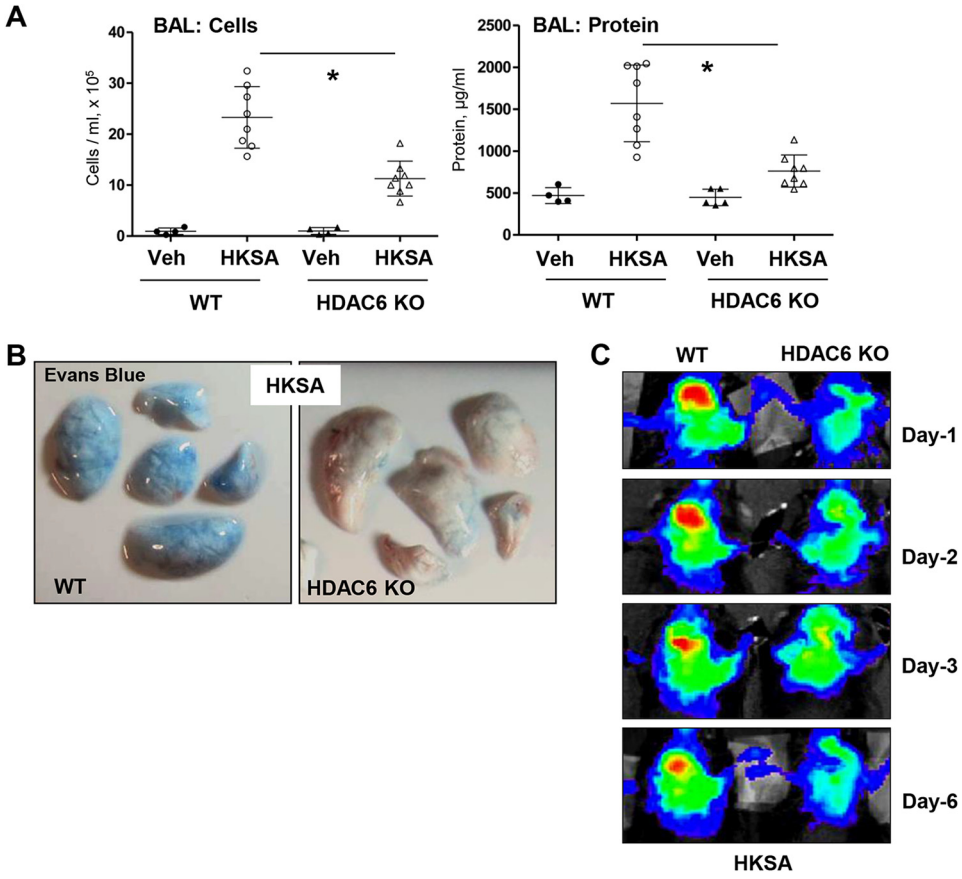

Figure 9. HKSA-induced lung inflammation is attenuated in HDAC6 knockout mice. WT C57BL/6 or HDAC6 KO mice were exposed to HKSA (2×10^8 bacterial cells/mouse, intratracheally) for 24 h. *A*, BAL was collected, and total cells and protein content were determined 24 h after HKSA administration. HDAC6 KO mice showed a significant decrease in protein content and cell counts in BAL. $n = 8$; *, $p < 0.05$. *Veh*, vehicle. *B*, analysis of Evans Blue–labeled albumin extravasation into the lung parenchyma. Lungs from HKSA-challenged (24 h) WT and HDAC6 KO mice were excised from the chest, perfused with PBS, and imaged. Shown are representative single-animal images from three independent experiments. Six total animals/condition were analyzed. *C*, live imaging analysis of lung vascular barrier dysfunction after HKSA intratracheal injection in WT and HDAC6 KO mice. HKSA-induced accumulation of fluorescent Angiosense 680 EX imaging agent in the lungs of the same animals was detected using a Xenogen IVIS 200 Spectrum imaging system at 1, 2, 3, and 6 days after HKSA challenge and presented in arbitrary *colors*. Shown are representative single-animal images from three independent experiments. Six total animals/condition were analyzed.

These findings also contribute to the current knowledge of the role of redox signaling in epigenetic regulation. Another study demonstrates ROS-mediated activation of another member of the HDAC family, HDAC3, during LPS challenge in cardiomyocytes (49).

The results of our study reveal the two separate mechanisms, EC barrier disruption and inflammation, caused by HKSA-induced MT destabilization. As a first mechanism, the partial disassembly of peripheral MT impairs the delivery of CLASP2 to the cell periphery, where it interacts with AJ proteins to enhance barrier integrity. The compromised interaction between CLASP2 and AJ proteins VE-cadherin and p120 catenin suppresses AJ assembly, thereby increasing EC permeability. As a second mechanism, HKSA–HDAC6 –induced MT disassembly leads to the release of MT-bound GEF-H1, which activates the Rho pathway of EC barrier dysfunction and leads to the additional activation of the NF-κB inflammatory cascade.

MT-associated proteins play a role in the agonist-induced regulation of MT dynamics and endothelial barrier, as shown in our previous reports (19, 51, 52). CLASP proteins represent a group of MT plus-end– binding proteins that provide structural links and maintain a dynamic interaction between the MT and actin cytoskeleton (53). CLASP2, via direct interaction with p120 catenin, may also regulate AJ functions and increase MT stability at the cell cortical compartment (36).

Published studies demonstrate a rapid disassembly of AJ and MT destabilization in the vascular EC following inflammatory insult. The disassembly of AJ complexes and accordingly CLASP2 dissociation from AJ may be initiated by different stimuli, including ROS-mediated phosphorylation of VE-cadherin, which occurs in a minute time frame (50). On the other hand, CLASP2 is delivered by growing MT to the AJ, where it participates in MT anchoring at the cell periphery, thus contributing to the stabilization of the peripheral MT. Interestingly, MT stabilization by Taxol partially attenuates both EC barrier dysfunction and the disassembly of AJ complexes caused by LPS (19). Our results show that loss of peripheral CLASP2 exerted a pronounced negative effect on EC barrier function, but this was partially restored by inhibition of HDAC6, which suggests that HDAC6 activation-led MT disruption affects AJ assembly, ultimately resulting in EC barrier disruption. Taken together, these data suggest a positive feedback regulation of AJ integrity by MT. We speculate that eventually both events contribute to vascular endothelium

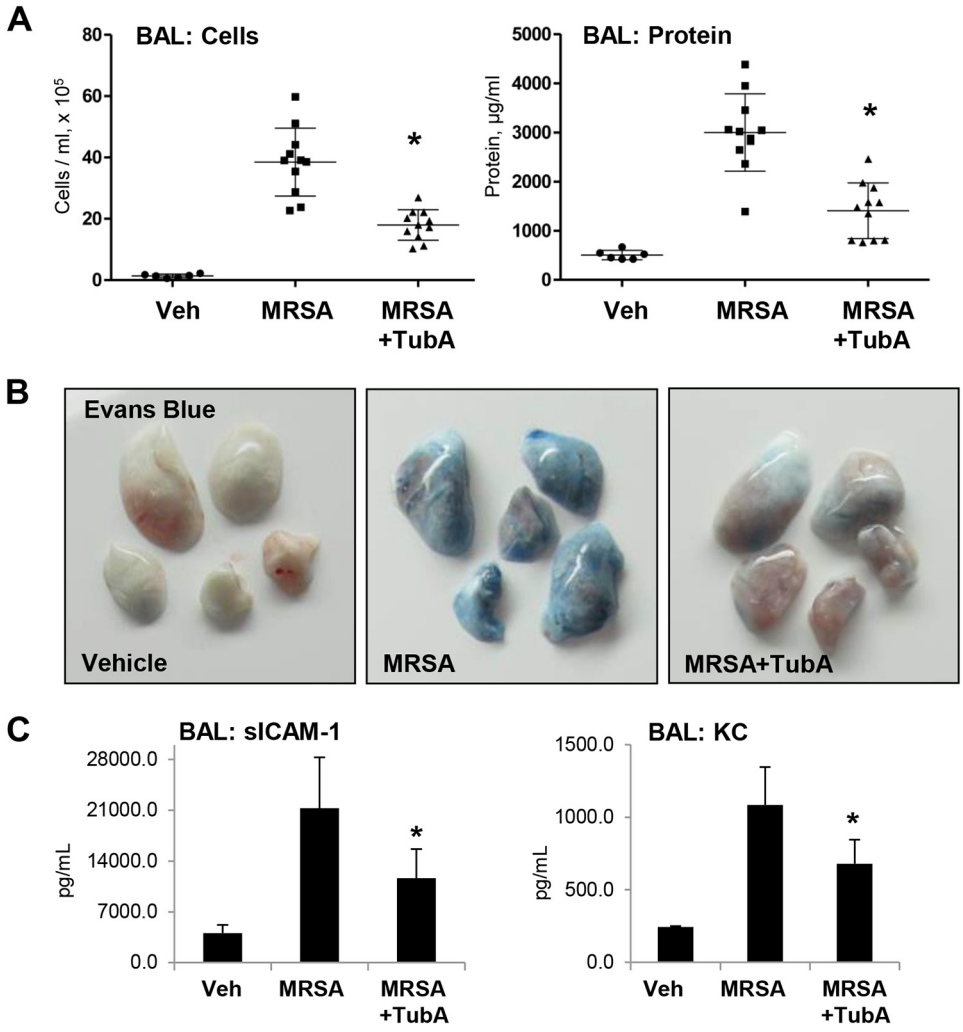

Figure 10. HDAC6 inhibitor TubA ameliorates MRSA-induced lung inflammation in mice. MRSA (CR-MRSA USA300, clinical strain 923) was injected into mice (1×10^8 cells/mouse, intratracheally) with or without intravenous administration of TubA (40 mg/kg). Control groups received saline, and mice were sacrificed after 24 h. *A*, BAL was collected from the mice followed by the determination of total cells and protein content. $n = 11$; *, $p < 0.05$. *Veh*, vehicle. *B*, analysis of Evans Blue–labeled albumin extravasation into the lung parenchyma. Lungs from MRSA-challenged (24 h) WT and HDAC6 KO mice with and without TubA co-treatment were excised from the chest, perfused with PBS, and imaged. Shown are representative single-animal images from three independent experiments. Eight total animals/condition were analyzed. *C*, the levels of soluble ICAM-1 and cytokine KC in BAL samples were determined by ELISA. $n = 4$/condition; *, $p < 0.05$.

dysfunction under inflammatory conditions. However, further studies are needed to determine whether AJ disassembly precedes the HKSA-induced CLASP2-mediated MT destabilization or disruption of the MT network is a primary event leading to AJ disassembly from loss of the membrane-bound CLASP2.

As mentioned above, the second pathway of EC permeability and inflammation caused by HKSA is a release and activation of GEF-H1 following agonist-induced MT depolymerization. Studies by our and other groups have shown that the release of MT-bound GEF-H1 leads to the activation of RhoA and its downstream signaling pathways (24, 25, 54, 55). Here, we show that HKSA-induced GEF-H1 release and activation depend on HDAC6 activity. The activation of RhoA signaling augmented HKSA-induced EC inflammatory activation and increased permeability. In turn, HDAC6 inhibition partially stabilized MT, attenuated RhoA signaling, and suppressed HKSA-induced expression of adhesion molecules ICAM-1 and VCAM-1 and proinflammatory cytokines. The requirement for HDAC6 activation in this process was further supported by the finding that EC with ectopic expression of WT HDAC6 responded to HKSA challenge with higher levels of NF-κB activation and ICAM-1 and VCAM-1 expression than cells with ectopic expression of the catalytically deficient HDAC6 mutant. The "MT–GEF-H1–inflammation" axis was further confirmed by experiments with siRNA-mediated depletion of GEF-H1, which inhibited HKSA-caused activation of NF-κB and the subsequent elevation of VCAM-1. We also cannot exclude other mechanisms of HDAC6-induced RhoA pathway activation. For example, inhibition of HDAC6 or HDAC3 has been shown to protect LPS-induced endothelial dysfunction and ALI by suppressing HSP90-mediated Rho activation (56).

It is also important to note that treatment with the HDAC6 inhibitor TubA resulted in complete rescue of acetylated tubulin in HKSA-challenged cells but only partially attenuated HKSA-induced endothelial cell permeability, activation of NF-κB signaling, and expression of inflammatory cytokines and adhesion molecules. How can these apparent discrepancies be

reconciled? The primary mechanism of EC inflammation caused by microbial components involves HKSA interaction with Toll-like receptors 2 and 4 (TLR2/4) resulting in the recruitment of TIR domain–containing adaptors MyD88, TIRAP, and TRIF to the cytoplasmic TLR domains called TIR domains. MyD88 is essential for the induction of inflammatory cytokines triggered by all TLR, and TIRAP is involved specifically in the MyD88-dependent pathway via TLR2 and TLR4 (57). Downstream, TLR activation triggers phosphorylation/activation of mitogen-activated protein kinases p42/p44, JNK1/2, and p38 and the activation of NF-κB cascade following NF-κB translocation to the nucleus (58, 59). However, NF-κB signaling is additionally regulated by RhoA activity, leading to amplification of inflammatory response (60). The results of the current study show that MT destabilization by activated HDAC6 in HKSA-challenged pulmonary EC stimulates RhoA signaling via a GEF-H1–dependent mechanism. This auxiliary stimulation of the NF-κB cascade by the GEF-H1–RhoA axis was abolished by MT stabilization with HDAC6 inhibitor TubA, whereas the priming TLR–MyD88–NF-κB inflammatory mechanism was not affected. Collectively, these findings demonstrate the existence of both MT-dependent and -independent mechanisms of inflammation triggered by HKSA.

The role of HDAC6-regulated MT dynamics in SA-induced lung barrier dysfunction and inflammation was further evaluated using animal models of HKSA- and MRSA-induced ALI. Some HDAC inhibitors have also been successfully employed to alleviate various animal models of lung injury (29, 61, 62). The data showed protective effects of TubA in both models of ALI caused by intratracheal instillation of heat-inactivated SA and a more clinically relevant MRSA isolate. The role of the HDAC6 mechanism in the propagation of HKSA-induced lung dysfunction was further supported by marked attenuation of HKSA-induced lung injury and inflammation in HDAC6 knockout mice.

In summary, this study describes a HDAC6–MT–associated signaling axis that promotes HKSA/MRSA-induced lung injury and inflammation. Based on our results, we propose a mechanistic model of HKSA-induced and HDAC6–MT—Rho-mediated lung injury, where SA infections trigger the generation of ROS leading to HDAC6 activation, which results in the destabilization of MT by tubulin deacetylation (Fig. 11). The destabilized MT ultimately cause EC permeability by activating RhoA signaling, weakening AJ assembly and impaired delivery of barrier-protective signaling molecules. HKSA-induced MT destabilization mediated by HDAC6 also promotes inflammation via GEF-H1—RhoA–induced augmentation of NF-κB inflammatory cascade. The *in vivo* efficacy of tubastatin A in protecting MRSA-induced lung injury underscores the potential of HDAC6 inhibitors as future alternative approaches to the treatment of antibiotic-resistant SA isolate–induced infections. Thus, MT stabilization or prevention of increased MT instability under pathologic conditions may represent an important therapeutic option aimed at the restoration of the healthy "signaling homeostasis" of cytoskeleton-associated networks.

Experimental procedures

Cell culture and reagents

HPAEC, culture medium, and growth supplements were obtained from Lonza (Allendale, NJ). Cells cultured following the manufacturer's instructions were used at passages 5–8. HKSA was purchased from InvivoGen (San Diego, CA). ICAM1 and VCAM1 antibodies were obtained from Santa Cruz Biotechnology (Santa Cruz, CA); β-actin, α-, β-, and acetylated tubulin antibodies were from Sigma; diphospho-MLC (myosin light chain), phospho-NF-κB, IκBα, and HDAC6 antibodies were obtained from Cell Signaling (Beverly, MA); CLASP2, VE-cadherin, and p120 catenin antibodies were from BD Transduction Laboratories (San Diego, CA). Texas Red phalloidin and Alexa Fluor 488–conjugated secondary antibodies were purchased form Molecular Probes (Eugene, OR). Unless specified, all other biochemical reagents were obtained from Sigma.

Measurement of endothelial permeability

Barrier integrity across the HPAEC monolayer was determined by measuring transendothelial electrical resistance using an electric cell–substrate impedance–sensing system, ECIS Z (Applied Biophysics, Troy, NY) as described earlier (54). Experiments were conducted only on wells that achieved >1200 ohms (10 microelectrodes/well) of steady state resistance. Resistance was expressed by the in-phase voltage (proportional to the resistance), which was normalized to the initial voltage and expressed as a fraction of the normalized resistance value. In the current studies, we did not observe significant effects of nonspecific RNA or specific siRNA on cell viability and monolayer integrity. Initial testing of nontransfected and siRNA-transfected EC monolayers did not reveal significant differences in basal TER levels. Endothelial permeability to macromolecules was monitored by express permeability visualization assay (Millipore catalog No. 17-10398) described elsewhere (38). After washing unbound FITC–avidin, the fluorescence of matrix-bound FITC–avidin in control and agonist-treated EC monolayers was measured on a Victor X5 multilabel plate reader (PerkinElmer).

Immunocytochemistry

HPAEC monolayers were plated on glass coverslips for immunofluorescence staining. Cells were fixed in 3.7% formaldehyde and permeabilized with 0.1% Triton X-100 in PBS-Tween (PBST) for 30 min at room temperature followed by blocking with 2% BSA in PBST for 30 min. Incubations with antibodies of interest were performed in blocking solution (2% BSA in PBST) for 1 h at room temperature followed by staining with Alexa-488– or Alexa-544–conjugated secondary antibodies. After immunostaining, the slides were analyzed using an EVOS FL Auto 2 cell imaging system (Thermo Fisher Scientific). Quantitative analysis of paracellular gap formation was performed as described previously (18, 22).

Western blotting and co-immunoprecipitation

Proteins were separated by SDS-PAGE and transferred to polyvinylidene difluoride membranes, which were incubated with the desired primary antibodies at 4 °C overnight. After incubation with horseradish peroxidase–conjugated secondary antibodies at

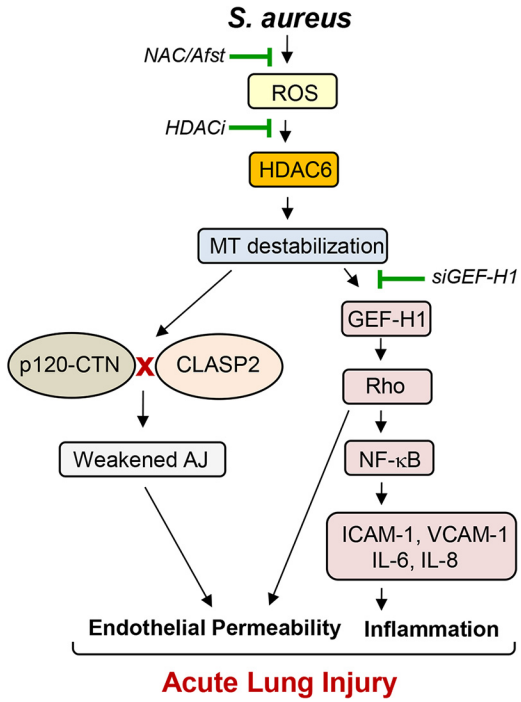

Figure 11. Proposed model HDAC6-dependent regulation of HKSA-induced EC permeability and inflammation. *S. aureus* infections generate ROS, which activates HDAC6, causing MT destabilization. Disassembly of peripheral MT structure and inhibition of MT growth to the cell periphery compromises delivery of MT-associated protein CLASP2 and its interaction with AJ proteins, leading to decreased AJ assembly and increased EC permeability. Concurrently, GEF-H1 released from destabilized MT evokes inflammation via the RhoA-dependent augmentation of NF-κB inflammatory cascade. RhoA also directly increases endothelial permeability via activation of actin cytoskeletal remodeling and actomyosin contractile mechanisms. ROS scavengers or pharmacological or genetic inhibitors of HDAC6 rescue HKSA/MRSA-induced EC permeability and inflammation by enhancing stability of MT cytoskeleton and promoting MT-dependent mechanisms of barrier protection.

room temperature for 1 h, membranes were developed using enhanced chemiluminescence substrate (Thermo Fisher Scientific). Equal protein loading was verified by probing the membranes with α-tubulin or β-tubulin antibody. For co-immunoprecipitation studies, the cells were lysed on ice with cold TBS–NP40 lysis buffer (20 mM Tris, pH 7.4, 150 mM NaCl, and 1% Nonidet P-40) supplemented with protease and phosphatase inhibitor cocktails (Roche Diagnostics). Clarified lysates were then incubated with specific antibodies of interest overnight at 4 °C followed by a 1-h incubation with protein G–agarose beads. After washing 3–4 times with TBS–NP40 lysis buffer, the complexes were analyzed by Western blotting using the appropriate antibodies. The relative intensities of the protein bands were quantified by scanning densitometry using ImageQuant software (GE Healthcare).

Subcellular fractionation

To isolate the microtubule-enriched fraction, human pulmonary EC monolayers were stimulated with HKSA and microtubule-enriched fractions were isolated as described previously (44). The levels of tubulin in the microtubule-enriched fractions from control and stimulated EC were evaluated by immunoblotting with α-tubulin antibodies. In fractionation studies, cytosolic (soluble) and membrane/cytoskeletal (particulate) fractions were isolated as described previously (63). Protein extracts were separated by SDS-PAGE, transferred to a polyvinylidene difluoride membranes, and probed with specific antibodies. In all experiments, the total cell lysates were normalized by loading equal protein amounts per lane as monitored by protein measurements in SDS samples. Reprobing the total lysate samples with antibody to α-tubulin or a particular protein of interest served as additional normalization controls.

RhoA and GEF-H1 activity assays

Active (GTP-bound) RhoA was captured using GST–rhotekin beads as previously reported (64). Briefly, HPAEC grown to confluence on 60-mm dishes and stimulated with HKSA were lysed with ice-cold Rho assay buffer containing 100 mM NaCl, 50 mM Tris-HCl, pH 7.6, 20 mM NaF, 10 mM $MgCl_2$, 1% Triton X-100, 0.5% deoxycholic acid, 0.1% SDS, 1 mM Na_3VO_4, and protease inhibitors. After a centrifugation step, the supernatants were incubated at 4 °C for 45 min with 20–25 μg of GST–rhotekin beads. Total cell lysates and the rhotekin-captured proteins following the bead-washing step were analyzed by Western blotting using RhoA antibody. Active GEF-H1 was affinity-precipitated from cell lysates as described previously (65) using a RhoA(G17A) mutant, which cannot bind nucleotide and therefore has high affinity for activated GEF (66). Activated GEF-H1 in RhoA (G17A) pulldowns was detected by immunoblotting and normalized to total GEF-H1 in cell lysates for each sample.

Surface protein biotinylation

Control and agonist-treated cells were washed with PBS at 37 °C and incubated for 10 min with 5 mM sulfo-NHS-SS-biotin (Pierce Biotechnology) at room temperature. After washing twice with ice-cold PBS containing 100 mM glycine, the cells were lysed for 30 min on ice in 1% Triton X-100–PBS and centrifuged at 10,000 × *g* for 10 min at 4 °C. Equal amounts of cell lysates were incubated with 60 μl of streptavidin–agarose (Pierce Biotechnology) for 1 h at 4 °C. Beads were washed three times with ice-cold PBS and boiled in SDS sample buffer with 5% 2-mercaptoethanol. Samples were centrifuged for 1 min at 1000 × *g*, and supernatants were subjected to Western blot analysis with VE-cadherin antibody.

Measurement of cytokines and HDAC6 activity

The cytokine levels in conditioned media from cells or BAL fluid from mouse lungs were determined using ELISA kits available from R&D Systems (Minneapolis, MN) according to the manufacturer's instructions. HDAC6 activity was measured using a fluorogenic HDAC6 assay kit available from BPS Bioscience (San Diego, CA) following the manufacturer's instructions.

siRNA and DNA transfections

For knockdown of HDAC6, GEF-H1, or CLASP2 in human pulmonary EC cultures, predesigned human siRNA were ordered from Ambion (Austin, TX) in purified, desalted, deprotected, and annealed double-strand form. Transfection of EC with siRNA was performed as described previously (67). After 72 h of transfection, cells were used for experiments or harvested for Western blotting verification of specific protein depletion. Nonspecific RNA (Dharmacon, Lafayette, CO) was

used as a control treatment. Plasmids encoding human WT and CD-HDAC6 proteins bearing a GFP tag were obtained from Addgene (Cambridge, MA) and used for transient transfections according to protocols described previously (18, 55). Control transfections were performed with empty vectors. After 24–48 h of transfection, cells were treated with the agonist of interest and used for permeability measurements or immunostaining.

Animal studies

All experimental protocols involving the use of animals were approved by the Institutional Animal Care and Use Committees of the University of Chicago and the University of Maryland. Briefly, 8–10-week–old C57BL/6J mice were anesthetized with an intraperitoneal injection of ketamine (75 mg/kg) and xylazine (7.5 mg/kg). Then, sterile saline solution, 2×10^8 bacterial cells of HKSA/mouse, or 1×10^8 MRSA (CR-MRSA USA300, clinical strain 923) was injected intratracheally using a 20-guage catheter. Immediately after the HKSA or MRSA injection, 10 mg/kg tubastatin A was injected intravenously, and after 24 h the animals were sacrificed by exsanguination under anesthesia. HDAC6-null mice were kindly provided by Timothy McKinsey (University of Colorado, Denver) (68).

Evaluation of lung injury parameters

After intratracheal injection of 1 ml of sterile Hanks' balanced salt buffer, BAL was carried out, and total protein and cells content were measured as described previously (69). To analyze vascular leak, Evans Blue dye (30 mg/kg) was injected into the external jugular vein 2 h before the end of the experiment, as described elsewhere (69).

For *in vivo* optical imaging, at specified times after challenge with HKSA or vehicle, mice were injected via the tail vein with 100 μl of 2 nmol Angiosense 680 EX imaging agent (Perkin-Elmer, catalog No. NEV10054EX). After 24 h, fluorescent optical imaging was performed using an Xenogen IVIS 200 Spectrum (Caliper Life Sciences, Alameda, CA). Mice were exposed to isoflurane anesthesia with O_2 through the gas anesthesia manifold and placed on the imaging stage. Acquisition and image analysis were performed with Living Image 4.3.1 software as we described previously (70).

Statistical analysis

Results are expressed as means ± S.D. of three to six independent experiments. The comparison between controls and stimulated groups was done by unpaired Student's *t* test or one-way ANOVA followed by Tukey's post hoc test, with $p < 0.05$ considered statistically significant.

Author contributions—P. K., Y. K., Y. T., T. O., A. S., N. S., C. P. M., and A. A. B. formal analysis; P. K., Y. K., Y. T., T. O., A. S., N. S., and C. P. M. validation; P. K., Y. K., Y. T., T. O., A. S., N. S., C. P. M., and A. A. B. investigation; P. K., Y. K., and T. O. visualization; P. K., Y. K., Y. T., T. O., A. S., and C. P. M. methodology; P. K. and A. A. B. writing-original draft; P. K., Y. K., and A. A. B. writing-review and editing; Y. K., A. S., and A. A. B. data curation; C. P. M. resources; C. P. M. and A. A. B. supervision; A. A. B. conceptualization; A. A. B. funding acquisition; A. A. B. project administration.

References

1. Mayr, F. B., Yende, S., and Angus, D. C. (2014) Epidemiology of severe sepsis. *Virulence* **5,** 4–11 CrossRef Medline
2. Heron, M. (2016) Deaths: Leading causes for 2014. *Natl. Vital Stat. Rep.* **65,** 1–96
3. Johnson, E. R., and Matthay, M. A. (2010) Acute lung injury: Epidemiology, pathogenesis, and treatment. *J. Aerosol Med. Pulm. Drug Deliv.* **23,** 243–252 CrossRef Medline
4. Woske, H. J., Röding, T., Schulz, I., and Lode, H. (2001) Ventilator-associated pneumonia in a surgical intensive care unit: Epidemiology, etiology and comparison of three bronchoscopic methods for microbiological specimen sampling. *Crit. Care* **5,** 167–173 CrossRef Medline
5. Paulsen, J., Mehl, A., Askim, Å., Solligård, E., Åsvold, B. O., and Damås, J. K. (2015) Epidemiology and outcome of *Staphylococcus aureus* bloodstream infection and sepsis in a Norwegian county 1996–2011: An observational study. *BMC Infect. Dis.* **15,** 116 CrossRef Medline
6. Wu, T., Xing, J., and Birukova, A. A. (2013) Cell-type-specific crosstalk between p38 MAPK and Rho signaling in lung micro- and macrovascular barrier dysfunction induced by *Staphylococcus aureus*-derived pathogens. *Transl. Res.* **162,** 45–55 CrossRef Medline
7. Xing, J., Moldobaeva, N., and Birukova, A. A. (2011) Atrial natriuretic peptide protects against *Staphylococcus aureus*-induced lung injury and endothelial barrier dysfunction. *J. Appl. Physiol.* (*1985*) **110,** 213–224Medline
8. Meliton, A. Y., Meng, F., Tian, Y., Sarich, N., Mutlu, G. M., Birukova, A. A., and Birukov, K. G. (2015) Oxidized phospholipids protect against lung injury and endothelial barrier dysfunction caused by heat-inactivated *Staphylococcus aureus*. *Am. J. Physiol. Lung Cell. Mol. Physiol.* **308,** L550–L562 CrossRef Medline
9. Tian, Y., Mambetsariev, I., Sarich, N., Meng, F., and Birukova, A. A. (2015) Role of microtubules in attenuation of PepG-induced vascular endothelial dysfunction by atrial natriuretic peptide. *Biochim. Biophys. Acta* **1852,** 104–119 CrossRef Medline
10. Spindler, V., Schlegel, N., and Waschke, J. (2010) Role of GTPases in control of microvascular permeability. *Cardiovasc. Res.* **87,** 243–253 CrossRef Medline
11. Vandenbroucke, E., Mehta, D., Minshall, R., and Malik, A. B. (2008) Regulation of endothelial junctional permeability. *Ann. N.Y. Acad. Sci.* **1123,** 134–145 CrossRef Medline
12. Anwar, K. N., Fazal, F., Malik, A. B., and Rahman, A. (2004) RhoA/Rho-associated kinase pathway selectively regulates thrombin-induced intercellular adhesion molecule-1 expression in endothelial cells via activation of IκB kinase β and phosphorylation of RelA/p65. *J. Immunol.* **173,** 6965–6972 CrossRef Medline
13. Guo, F., Tang, J., Zhou, Z., Dou, Y., Van Lonkhuyzen, D., Gao, C., and Huan, J. (2012) GEF-H1-RhoA signaling pathway mediates LPS-induced NF-κB transactivation and IL-8 synthesis in endothelial cells. *Mol. Immunol.* **50,** 98–107 CrossRef Medline
14. Shimada, H., and Rajagopalan, L. E. (2010) Rho kinase-2 activation in human endothelial cells drives lysophosphatidic acid-mediated expression of cell adhesion molecules via NF-κB p65. *J. Biol. Chem.* **285,** 12536–12542 CrossRef Medline
15. Akhshi, T. K., Wernike, D., and Piekny, A. (2014) Microtubules and actin crosstalk in cell migration and division. *Cytoskeleton* (*Hoboken*) **71,** 1–23Medline
16. Alieva, I. B., Zemskov, E. A., Smurova, K. M., Kaverina, I. N., and Verin, A. D. (2013) The leading role of microtubules in endothelial barrier dysfunction: Disassembly of peripheral microtubules leaves behind the cytoskeletal reorganization. *J. Cell. Biochem.* **114,** 2258–2272 CrossRef Medline
17. Nogales, E. (2000) Structural insights into microtubule function. *Annu. Rev. Biochem.* **69,** 277–302 CrossRef Medline
18. Birukova, A. A., Birukov, K. G., Smurova, K., Adyshev, D., Kaibuchi, K., Alieva, I., Garcia, J. G., and Verin, A. D. (2004) Novel role of microtubules in thrombin-induced endothelial barrier dysfunction. *FASEB J.* **18,** 1879–1890 CrossRef Medline

19. Kratzer, E., Tian, Y., Sarich, N., Wu, T., Meliton, A., Leff, A., and Birukova, A. A. (2012) Oxidative stress contributes to lung injury and barrier dysfunction via microtubule destabilization. *Am. J. Respir. Cell Mol. Biol.* **47,** 688–697 CrossRef Medline
20. Petrache, I., Birukova, A., Ramirez, S. I., Garcia, J. G., and Verin, A. D. (2003) The role of the microtubules in tumor necrosis factor-α-induced endothelial cell permeability. *Am. J. Respir. Cell Mol. Biol.* **28,** 574–581 CrossRef Medline
21. Birukova, A. A., Birukov, K. G., Adyshev, D., Usatyuk, P., Natarajan, V., Garcia, J. G., and Verin, A. D. (2005) Involvement of microtubules and Rho pathway in TGF-β1-induced lung vascular barrier dysfunction. *J. Cell. Physiol.* **204,** 934–947 CrossRef Medline
22. Birukova, A. A., Smurova, K., Birukov, K. G., Usatyuk, P., Liu, F., Kaibuchi, K., Ricks-Cord, A., Natarajan, V., Alieva, I., Garcia, J. G., and Verin, A. D. (2004) Microtubule disassembly induces cytoskeletal remodeling and lung vascular barrier dysfunction: Role of Rho-dependent mechanisms. *J. Cell. Physiol.* **201,** 55–70 CrossRef Medline
23. Verin, A. D., Birukova, A., Wang, P., Liu, F., Becker, P., Birukov, K., and Garcia, J. G. (2001) Microtubule disassembly increases endothelial cell barrier dysfunction: role of MLC phosphorylation. *Am. J. Physiol. Lung Cell. Mol. Physiol.* **281,** L565–L574 CrossRef Medline
24. Krendel, M., Zenke, F. T., and Bokoch, G. M. (2002) Nucleotide exchange factor GEF-H1 mediates cross-talk between microtubules and the actin cytoskeleton. *Nat. Cell Biol.* **4,** 294–301 CrossRef Medline
25. Chang, Y. C., Nalbant, P., Birkenfeld, J., Chang, Z. F., and Bokoch, G. M. (2008) GEF-H1 couples nocodazole-induced microtubule disassembly to cell contractility via RhoA. *Mol. Biol. Cell* **19,** 2147–2153 CrossRef Medline
26. Matsuyama, A., Shimazu, T., Sumida, Y., Saito, A., Yoshimatsu, Y., Seigneurin-Berny, D., Osada, H., Komatsu, Y., Nishino, N., Khochbin, S., Horinouchi, S., and Yoshida, M. (2002) *In vivo* destabilization of dynamic microtubules by HDAC6-mediated deacetylation. *EMBO J.* **21,** 6820–6831 CrossRef Medline
27. Zilberman, Y., Ballestrem, C., Carramusa, L., Mazitschek, R., Khochbin, S., and Bershadsky, A. (2009) Regulation of microtubule dynamics by inhibition of the tubulin deacetylase HDAC6. *J. Cell Sci.* **122,** 3531–3541 CrossRef Medline
28. Saito, S., Lasky, J. A., Guo, W., Nguyen, H., Mai, A., Danchuk, S., Sullivan, D. E., and Shan, B. (2011) Pharmacological inhibition of HDAC6 attenuates endothelial barrier dysfunction induced by thrombin. *Biochem. Biophys. Res. Commun.* **408,** 630–634 CrossRef Medline
29. Ni, Y. F., Wang, J., Yan, X. L., Tian, F., Zhao, J. B., Wang, Y. J., and Jiang, T. (2010) Histone deacetylase inhibitor, butyrate, attenuates lipopolysaccharide-induced acute lung injury in mice. *Respir. Res.* **11,** 33 CrossRef Medline
30. Hubbert, C., Guardiola, A., Shao, R., Kawaguchi, Y., Ito, A., Nixon, A., Yoshida, M., Wang, X. F., and Yao, T. P. (2002) HDAC6 is a microtubule-associated deacetylase. *Nature* **417,** 455–458 CrossRef Medline
31. Gorshkov, B. A., Zemskova, M. A., Verin, A. D., and Bogatcheva, N. V. (2012) Taxol alleviates 2-methoxyestradiol-induced endothelial permeability. *Vascul. Pharmacol.* **56,** 56–63 CrossRef Medline
32. Bogatcheva, N. V., Adyshev, D., Mambetsariev, B., Moldobaeva, N., and Verin, A. D. (2007) Involvement of microtubules, p38, and Rho kinases pathway in 2-methoxyestradiol-induced lung vascular barrier dysfunction. *Am. J. Physiol. Lung Cell. Mol. Physiol.* **292,** L487–L499 CrossRef Medline
33. Maki, T., Grimaldi, A. D., Fuchigami, S., Kaverina, I., and Hayashi, I. (2015) CLASP2 has two distinct TOG domains that contribute differently to microtubule dynamics. *J. Mol. Biol.* **427,** 2379–2395 CrossRef Medline
34. Engel, U., Zhan, Y., Long, J. B., Boyle, S. N., Ballif, B. A., Dorey, K., Gygi, S. P., Koleske, A. J., and Vanvactor, D. (2014) Abelson phosphorylation of CLASP2 modulates its association with microtubules and actin. *Cytoskeleton* (*Hoboken*) **71,** 195–209 Medline
35. Lansbergen, G., Grigoriev, I., Mimori-Kiyosue, Y., Ohtsuka, T., Higa, S., Kitajima, I., Demmers, J., Galjart, N., Houtsmuller, A. B., Grosveld, F., and Akhmanova, A. (2006) CLASPs attach microtubule plus ends to the cell cortex through a complex with LL5β. *Dev. Cell* **11,** 21–32 CrossRef Medline
36. Shahbazi, M. N., Megias, D., Epifano, C., Akhmanova, A., Gundersen, G. G., Fuchs, E., and Perez-Moreno, M. (2013) CLASP2 interacts with p120-catenin and governs microtubule dynamics at adherens junctions. *J. Cell Biol.* **203,** 1043–1061 CrossRef Medline
37. Shahbazi, M. N., and Perez-Moreno, M. (2014) Microtubules CLASP to adherens junctions in epidermal progenitor cells. *Bioarchitecture* **4,** 25–30 CrossRef Medline
38. Dubrovskyi, O., Birukova, A. A., and Birukov, K. G. (2013) Measurement of local permeability at subcellular level in cell models of agonist- and ventilator-induced lung injury. *Lab. Invest.* **93,** 254–263 CrossRef Medline
39. Piperno, G., LeDizet, M., and Chang, X. J. (1987) Microtubules containing acetylated α-tubulin in mammalian cells in culture. *J. Cell Biol.* **104,** 289–302 CrossRef Medline
40. Fu, P., Murley, J. S., Grdina, D. J., Birukova, A. A., and Birukov, K. G. (2011) Induction of cellular antioxidant defense by amifostine improves ventilator-induced lung injury. *Crit. Care Med.* **39,** 2711–2721 CrossRef Medline
41. Kempe, S., Kestler, H., Lasar, A., and Wirth, T. (2005) NF-κB controls the global pro-inflammatory response in endothelial cells: Evidence for the regulation of a pro-atherogenic program. *Nucleic Acids Res.* **33,** 5308–5319 CrossRef Medline
42. Kolaczkowska, E., and Kubes, P. (2013) Neutrophil recruitment and function in health and inflammation. *Nat. Rev. Immunol.* **13,** 159–175 CrossRef Medline
43. Smurova, K. M., Biriukova, A. A., Verin, A. D., and Alieva, I. B. (2008) [The microtubule system in endothelial barrier dysfunction: Disassembly of peripheral microtubules and microtubules reorganization in internal cytoplasm]. [Article in Russian] *Tsitologiia* **50,** 49–55 Medline
44. Birukova, A. A., Birukov, K. G., Gorshkov, B., Liu, F., Garcia, J. G., and Verin, A. D. (2005) MAP kinases in lung endothelial permeability induced by microtubule disassembly. *Am. J. Physiol. Lung Cell Mol. Physiol.* **289,** L75–L84 CrossRef Medline
45. Li, L., Hu, J., He, T., Zhang, Q., Yang, X., Lan, X., Zhang, D., Mei, H., Chen, B., and Huang, Y. (2015) P38/MAPK contributes to endothelial barrier dysfunction via MAP4 phosphorylation-dependent microtubule disassembly in inflammation-induced acute lung injury. *Sci. Rep.* **5,** 8895 CrossRef Medline
46. McLoughlin, A., Rochfort, K. D., McDonnell, C. J., Kerrigan, S. W., and Cummins, P. M. (2017) *Staphylococcus aureus*-mediated blood-brain barrier injury: An *in vitro* human brain microvascular endothelial cell model. *Cell. Microbiol.* **19** CrossRef Medline
47. Pai, A. B., Patel, H., Prokopienko, A. J., Alsaffar, H., Gertzberg, N., Neumann, P., Punjabi, A., and Johnson, A. (2012) Lipoteichoic acid from *Staphylococcus aureus* induces lung endothelial cell barrier dysfunction: Role of reactive oxygen and nitrogen species. *PLoS ONE* **7,** e49209 CrossRef Medline
48. Borgas, D., Chambers, E., Newton, J., Ko, J., Rivera, S., Rounds, S., and Lu, Q. (2016) Cigarette smoke disrupted lung endothelial barrier integrity and increased susceptibility to acute lung injury via histone deacetylase 6. *Am. J. Respir. Cell Mol. Biol.* **54,** 683–696 CrossRef Medline
49. Zhu, H., Shan, L., Schiller, P. W., Mai, A., and Peng, T. (2010) Histone deacetylase-3 activation promotes tumor necrosis factor-α (TNF-α) expression in cardiomyocytes during lipopolysaccharide stimulation. *J. Biol. Chem.* **285,** 9429–9436 CrossRef Medline
50. Birukova, A. A., Starosta, V., Tian, X., Higginbotham, K., Koroniak, L., Berliner, J. A., and Birukov, K. G. (2013) Fragmented oxidation products define barrier disruptive endothelial cell response to OxPAPC. *Transl. Res.* **161,** 495–504 CrossRef Medline
51. Tian, X., Tian, Y., Sarich, N., Wu, T., and Birukova, A. A. (2012) Novel role of stathmin in microtubule-dependent control of endothelial permeability. *FASEB J.* **26,** 3862–3874 CrossRef Medline
52. Tian, Y., Tian, X., Gawlak, G., O'Donnell, J.J., 3rd, Sacks, D. B., and Birukova, A. A. (2014) IQGAP1 regulates endothelial barrier function via EB1-cortactin cross talk. *Mol. Cell. Biol.* **34,** 3546–3558 CrossRef Medline
53. Tsvetkov, A. S., Samsonov, A., Akhmanova, A., Galjart, N., and Popov, S. V. (2007) Microtubule-binding proteins CLASP1 and CLASP2 interact with actin filaments. *Cell Motil. Cytoskeleton* **64,** 519–530 CrossRef Medline

54. Birukova, A. A., Adyshev, D., Gorshkov, B., Bokoch, G. M., Birukov, K. G., and Verin, A. D. (2006) GEF-H1 is involved in agonist-induced human pulmonary endothelial barrier dysfunction. *Am. J. Physiol. Lung Cell. Mol. Physiol.* **290,** L540–L548 CrossRef Medline
55. Birukova, A. A., Fu, P., Xing, J., Yakubov, B., Cokic, I., and Birukov, K. G. (2010) Mechanotransduction by GEF-H1 as a novel mechanism of ventilator-induced vascular endothelial permeability. *Am. J. Physiol. Lung Cell. Mol. Physiol.* **298,** L837–L848 CrossRef Medline
56. Joshi, A. D., Barabutis, N., Birmpas, C., Dimitropoulou, C., Thangjam, G., Cherian-Shaw, M., Dennison, J., and Catravas, J. D. (2015) Histone deacetylase inhibitors prevent pulmonary endothelial hyperpermeability and acute lung injury by regulating heat shock protein 90 function. *Am. J. Physiol. Lung Cell. Mol. Physiol.* **309,** L1410–L1419 CrossRef Medline
57. Takeda, K., and Akira, S. (2004) TLR signaling pathways. *Semin. Immunol.* **16,** 3–9 CrossRef Medline
58. Arbibe, L., Mira, J. P., Teusch, N., Kline, L., Guha, M., Mackman, N., Godowski, P. J., Ulevitch, R. J., and Knaus, U. G. (2000) Toll-like receptor 2-mediated NF-κB activation requires a Rac1-dependent pathway. *Nat. Immunol.* **1,** 533–540 CrossRef Medline
59. Dauphinee, S. M., and Karsan, A. (2006) Lipopolysaccharide signaling in endothelial cells. *Lab. Invest.* **86,** 9–22 CrossRef Medline
60. Perez-Moreno, M., Davis, M. A., Wong, E., Pasolli, H. A., Reynolds, A. B., and Fuchs, E. (2006) p120-Catenin mediates inflammatory responses in the skin. *Cell* **124,** 631–644 CrossRef Medline
61. Cetinkaya, M., Cansev, M., Cekmez, F., Tayman, C., Canpolat, F. E., Kafa, I. M., Yaylagul, E. O., Kramer, B. W., and Sarici, S. U. (2015) Protective effects of valproic acid, a histone deacetylase inhibitor, against hyperoxic lung injury in a neonatal rat model. *PLoS ONE* **10,** e0126028 CrossRef Medline
62. Zhang, L., Jin, S., Wang, C., Jiang, R., and Wan, J. (2010) Histone deacetylase inhibitors attenuate acute lung injury during cecal ligation and puncture-induced polymicrobial sepsis. *World J. Surg.* **34,** 1676–1683 CrossRef Medline
63. Birukova, A. A., Malyukova, I., Poroyko, V., and Birukov, K. G. (2007) Paxillin-β-catenin interactions are involved in Rac/Cdc42-mediated endothelial barrier-protective response to oxidized phospholipids. *Am. J. Physiol. Lung Cell. Mol. Physiol.* **293,** L199–L211 CrossRef Medline
64. Birukova, A. A., Smurova, K., Birukov, K. G., Kaibuchi, K., Garcia, J. G., and Verin, A. D. (2004) Role of Rho GTPases in thrombin-induced lung vascular endothelial cells barrier dysfunction. *Microvasc. Res.* **67,** 64–77 CrossRef Medline
65. Kakiashvili, E., Speight, P., Waheed, F., Seth, R., Lodyga, M., Tanimura, S., Kohno, M., Rotstein, O. D., Kapus, A., and Szászi, K. (2009) GEF-H1 mediates tumor necrosis factor-α-induced Rho activation and myosin phosphorylation: Role in the regulation of tubular paracellular permeability. *J. Biol. Chem.* **284,** 11454–11466 CrossRef Medline
66. García-Mata, R., Wennerberg, K., Arthur, W. T., Noren, N. K., Ellerbroek, S. M., and Burridge, K. (2006) Analysis of activated GAPs and GEFs in cell lysates. *Methods Enzymol.* **406,** 425–437 CrossRef Medline
67. Birukova, A. A., Burdette, D., Moldobaeva, N., Xing, J., Fu, P., and Birukov, K. G. (2010) Rac GTPase is a hub for protein kinase A and Epac signaling in endothelial barrier protection by cAMP. *Microvasc. Res.* **79,** 128–138 CrossRef Medline
68. Demos-Davies, K. M., Ferguson, B. S., Cavasin, M. A., Mahaffey, J. H., Williams, S. M., Spiltoir, J. I., Schuetze, K. B., Horn, T. R., Chen, B., Ferrara, C., Scellini, B., Piroddi, N., Tesi, C., Poggesi, C., Jeong, M. Y., and McKinsey, T. A. (2014) HDAC6 contributes to pathological responses of heart and skeletal muscle to chronic angiotensin-II signaling. *Am. J. Physiol. Heart Circ. Physiol.* **307,** H252–H258 CrossRef Medline
69. Fu, P., Birukova, A. A., Xing, J., Sammani, S., Murley, J. S., Garcia, J. G., Grdina, D. J., and Birukov, K. G. (2009) Amifostine reduces lung vascular permeability via suppression of inflammatory signalling. *Eur. Respir. J.* **33,** 612–624 CrossRef Medline
70. Birukova, A. A., Meng, F., Tian, Y., Meliton, A., Sarich, N., Quilliam, L. A., and Birukov, K. G. (2015) Prostacyclin post-treatment improves LPS-induced acute lung injury and endothelial barrier recovery via Rap1. *Biochim. Biophys. Acta* **1852,** 778–791 CrossRef Medline